INTERNATIONAL ATOMIC ENERGY AGENCY
UNITED NATIONS EDUCATIONAL, SCIENTIFIC AND CULTURAL ORGANIZATION

INTERNATIONAL CENTRE FOR THEORETICAL PHYSICS
34100 TRIESTE (ITALY) - P.O.B. 586 - MIRAMARE - STRADA COSTIERA 11 - TELEPHONES: 224281/9/8/4/6/5/6
CABLE: CENTRATOM - TELEX 460392-1

SMR/115 - 20

WINTER COLLEGE ON LASERS, ATOMIC AND MOLECULAR PHYSICS

(21 January - 22 March 1985)

PICOSECOND AND FEMTOSECOND LASERS

S. DE SILVESTRI
Centro di Elettronica Quantistica
e Strumentazione Elettronica
Istituto di Fisica del Politecnico
Piazza Leonardo da Vinci, 32
20133 Milano
Italy

S. DE SILVESTRI

(1)

FROM:

E.P. IPPEN, "OPTO-ELECTRONICS",
ed. by K. YOUNG, (1983)

1. ULTRASHORT PULSE GENERATION AND PROPAGATION

1.1 Introduction

Short flashes of light have long provided a means for capturing events in time and for studying high speed motion (Shapiro, 1977). As shorter light pulses have become available, an increasing variety of physical phenomena have become amenable to study and new areas of research have opened up. Strobe photography, pioneered (Edgerton, 1932) in the early thirties, offers microsecond temporal resolution which can be used to freeze the most rapid mechanical motion of microscopic objects. Scientific use of these high speed flash techniques pushed ahead rapidly in the fifties after their usefulness for initiating and studying fast photo-chemical reactions was demonstrated (Porter, 1950). With the invention of the laser even more rapid advance occurred. The dramatic increases in optical intensity and monochromaticity made possible by lasers were accompanied by a shortening of pulse durations from the nanosecond (10^{-9} sec) to the picosecond (10^{-12} sec) regime. Exciting opportunities for accurate study of previously unresolved, fast photoprocesses in physics, chemistry and biology were opened up. The possibility of enormously expanding the bandwidth of communication technology was also recognized.

In the decade between 1965 and 1975 major advances were made in the measurement, control, and utilization of ultrashort light pulses. With measurement required on a timescale too fast for conventional electronics, new techniques had to be invented. Interestingly enough, as these new techniques have developed and as the scientific understanding of fast processes has improved, further progress in short pulse generation has been achieved. In 1974 the first pulses shorter than a picosecond (10^{-12} sec) were generated (Shank and Ippen, 1974) and just recently the 10^{-13} sec mark has been passed (Fork et al., 1981). As this is being written scientific investigations of a variety of high speed phenomena are being pursued into femtosecond (10^{-15} sec) domain. At the same

time, compact opto-electronic devices are being developed for the purpose of making picosecond signal processing and transmission a practical reality.

The progress in short pulse generation is illustrated graphically in Figure 1.1. Passive modelocking of the Nd:glass laser (DeMaria et al., 1966) first led to the generation of pulses less than 10 psec in duration. This achievement provided much of the stimulus for picosecond technological development in the next decade. During this time, because of the high peak powers it provided, the Nd:glass also remained the work-horse of the field. A well designed system can provide transform-limited pulses in the 3-6 psec range, although repetition rates remain very low.

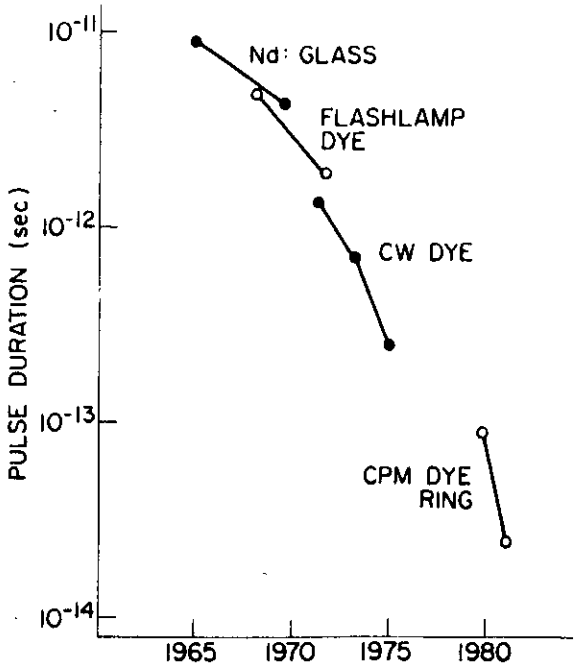

FIGURE 1.1 The decrease in optical pulsewidth as a function of time since 1965.

The passively-modelocked flashlamp-pumped dye laser (Schmidt and Schäfer, 1968; Bradley, 1977) provided both a decrease in pulsewidth and a broad extension of wavelength coverage. It was still a flashlamp system, subject to fluctuation and low repetition, but it generated pulses in a way that was fundamentally different from that of the Nd:glass laser. Streak camera investigations of ultrashort pulse formation in flashlamp-pumped dye lasers (Arthurs et al., 1973a; Arthurs et al., 1973b; Dempster et al., 1972) revealed that the mechanism of modelocking in dye lasers was different from that occuring in giant-pulse lasers. Rate equation analysis (New, 1974) confirmed that, in these lasers, the combined action of gain and absorber saturation can produce rapid pulse compression even in the absence of a fast response time in the absorber. It was this mechanism, then, that made possible the next generation of picosecond and subpicosecond sources: passively modelocked, continuously operated, dye lasers. With the first operation of such a cw system (Ippen et al., 1972) pulses as short as 1.5 psec were generated. Subsequent improvements and modifications of that system led to pulses as short as 0.3 psec (Ippen and Shank, 1975). More recently, with a bidirectional, colliding-pulse-modelocked (CPM) ring laser (Fork et al., 1981), pulse durations have moved below the 0.1 psec (100 fsec) mark. Further manipulation of these pulses by self-phase modulation in a short optical fiber and compression with a grating pair has produced pulses as short as 30 fsec (Shank et al., 1982).

Perhaps just as important as the ultrashort pulse durations are the reproducibility from pulse to pulse and the high repetition rates that are achieved with cw lasers. Powerful signal-averaging techniques can therefore be applied to picosecond and femtosecond studies and measurements can be made with low intensity pulses that do not distort the process under investigation. The decrease in "shortest" pulse duration documented in Figure 1.1 also does not indicate the variety of other new picosecond laser systems that have, during this same period, provided an

ever increasing wavelength coverage and measurement versatility. We discuss some of these in Chapter 2.

As optical pulse durations from lasers have decreased dramatically during the past decade so have the capabilities of optical transmission systems expanded enormously. Optical fibers with losses as low as 0.6 dB/km near 1.3 μm and 0.2 dB/km near 1.6 μm (Mija et al., 1979) are now available. Fiber dispersion, of primary importance for short pulse propagation, can also be minimized (or optimized for special cases) in this long wavelength regime. The predicted "zero-dispersion" behavior (Li, 1978) has been confirmed by pulse-delay measurements using wavelength-tunable radiation generated in a fiber by stimulated Raman effect (Cohen and Lin, 1977; Lin et al., 1978) and by the transmission of picosecond pulses over kilometer-lengths of single mode fiber without observable pulse broadening (Bloom et al., 1979). Recent work with double-clad single mode fibers (Mija et al., 1981; Jang et al., 1982) has produced fibers with two dispersion minima and a resulting low dispersion over a broad spectral range to accomodate use at both 1.3 μm and 1.6 μm. The chromatic dispersion of such a fiber is plotted in Figure 1.2 and compared with that of a conventional

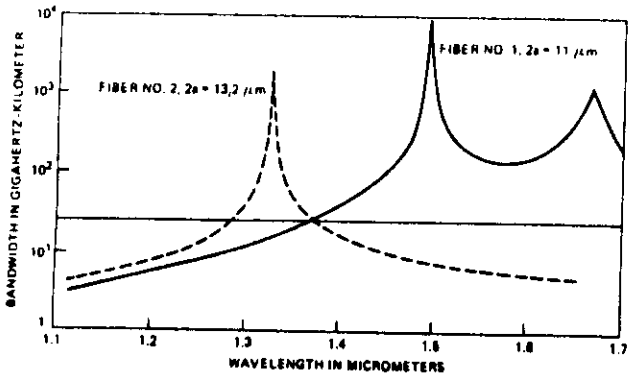

FIGURE 1.2 Transmission bandwidth of a double-clad single-mode fiber (Jang et al., 1982).

single mode fiber. From the point of view of sub-picosecond technology, it is interesting to note that within the range of 1.5 μm to 1.66 μm the dispersion of this fiber is less than 0.7 ps/km/nm. With additional tailoring the limit could be pushed well into the femtosecond regime.

1.2 Short Pulse Generation

The method by which short laser pulses are generated is called "modelocking" (Smith et al., 1975). That is: laser modes at different eigenfrequencies are locked together in phase to produce a coherent oscillation over the relatively broad band necessary for a short optical pulse. Although we shall see later that the most convenient treatments of short pulse formation and propagation rely on time domain analysis, a brief review of the frequency domain implications will also be helpful.

For each transverse (spatial) mode of a laser resonator there corresponds a set of longitudinal modes separated in frequency by $c/2L$, where c is the speed of light and L is the optical pathlength between the two mirrors. If the medium between the mirrors is dispersive, as it is in semiconductor diode laser for example, the spacing between resonator modes is more precisely:

$$\frac{c}{2n_g L} = \frac{c}{2L\left[n + \nu \frac{dn}{d\nu}\right]} \tag{1.1}$$

where c/n_g, the group velocity in the medium, is expressed in terms of the derivative of the index of refraction with respect to frequency ν. Note that for linear dispersion (i.e. $dn/d\nu$ = const.) the modes remain equally spaced.

Consider now the n-th mode to have amplitude E_n, angular frequency ω_n, and phase ϕ_n, then the total laser output field E_T can be written

$$E_T = \sum_n E_n \exp\{i[\omega_n(t - z/c) + \phi_n]\} + c.c. \qquad (1.2)$$

where c.c. represents the complex conjugate and the observed output is travelling in the positive z direction. With equal mode spacing $\omega_n = \omega_o + n\Delta$, where $\Delta = 2\pi(c/2L)$, we can write

$$E_T = \exp\{i\omega_o(t - z/c)\} \sum_n E_n \exp\{i[n\Delta(t - z/c) + \phi_n]\} + c.c. \qquad (1.3)$$

This corresponds to a carrier wave of frequency ω_o whose envelope is periodic with period $T = 2L/c$ and travels with the velocity c. For ϕ_n a constant (i.e. all phases locked together) the envelope consists of a single pulse per period with a pulsewidth given approximately by the reciprocal of the frequency range over which the E_n's have appreciable value. That is, the pulsewidth

$$t_p = \{N(c/2L)\}^{-1} \qquad (1.4)$$

where N is the number of oscillating modes. This frequency domain picture is illustrated in Figure 1.3. The larger the laser bandwidth, the shorter the potential pulse durations. Table I gives a rough indication of the available bandwidths in some of the most commonly mode-locked lasers. Actual pulseshapes depend upon the method of modelocking and a variety of material properties. Incomplete locking of modes results in an envelope

TABLE 1.1 Bandwidths of several common lasers

	$\Delta\nu$		$\Delta\tau$
HeNe	1 GHz		400 psec
ArgonIon	3 GHz		130 psec
Nd:YAG	10 GHz		30 psec
Nd:Glass	3,000 GHz		.25 psec
Semiconductor	10,000 GHz	(100 A°)	.05 psec
Dye	30,000 GHz	(300 A°)	.02 psec

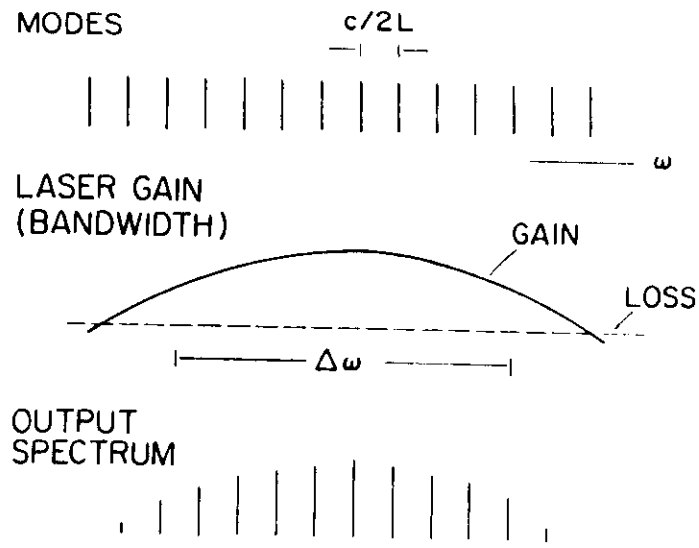

MODELOCKING

$$\Rightarrow \Delta t \cong \frac{1}{\Delta\omega} = \left(\frac{1}{N}\right)\left(\frac{2L}{c}\right)$$

WHERE N = # OF MODES LOCKED

FIGURE 1.3 Oscillating spectrum and potential pulse duration of a multi-longitudinal mode laser.

larger than that predicted by the oscillating mode spectrum. The minimum pulsewidth obtainable from a given mode spectrum is referred to as the Fourier transform-limited pulsewidth. When calculating this limit one should remember that the measurable quantity, spectral density, is not the Fourier transform of the intensity but rather of the electric field autocorrelation. If a pulse is to be considered 'transform limited' the time-bandwidth product must correspond to the minimum value for its particular pulse shape (see Chapter 3).

Techniques for producing modelocking fall into two categories as illustrated in Figure 1.4, active and passive. In active modelocking, loss or phase modulation is introduced into the laser

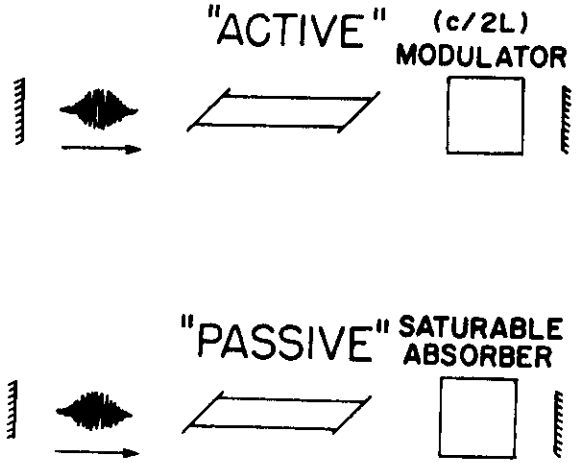

FIGURE 1.4 Schematic representations of active and passive pulse generation with an intracavity element near one end of the laser resonator.

resonator. If the modulation frequency is approximately equal to the mode frequency separation, the sidebands generated cause a phase locking to occur as illustrated in Figures 1.5 and 1.6. Such analysis can be difficult for many modes. An equally valid and more tractable approach is to consider the shaping that occurs as the pulse of light passes through the modulator each period near the point of minimum loss.

Passive modelocking involves the use of an intracavity saturable absorber that passes intense pulses of light with less loss than experienced by a constant low level of light. Under the proper conditions the laser output spontaneously breaks up into a train of "modelocked" pulses. The difference between active and passive modelocking is simply that, in the latter, the optical pulse provides its own modulation. Passive modelocking, when possible, generally results in the shortest pulses

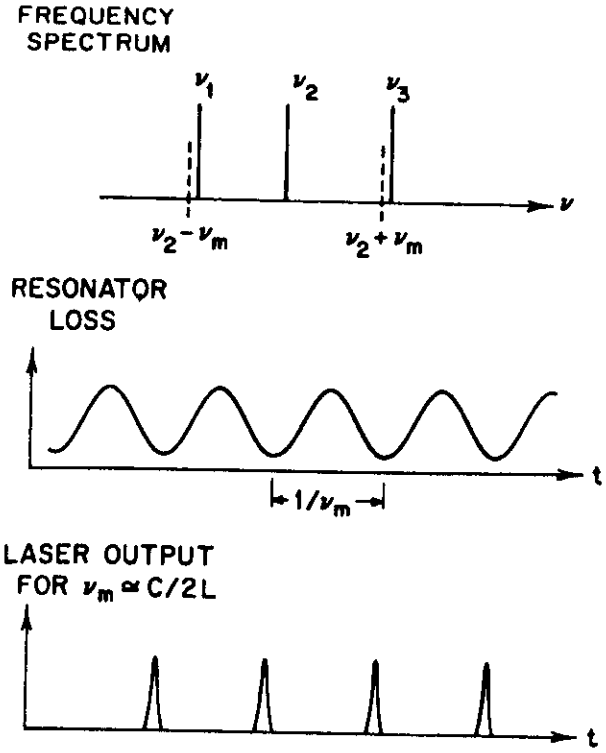

FIGURE 1.5 Loss modulation can be considered either as means of modelocking by sideband generation or by transmission gating.

obtainable with a given laser medium.

1.3 Active Modelocking

Much of the early theoretical work on modelocking focused on homogeneously broadened lasers with active, internal modulation. It was the first case to yield analytical solutions for steady state pulse shapes and pulse duration (Kuizenga and Siegman, 1970a). For homogeneous broadening and long upper-state life-time (appropriate to solid-state lasers like Nd:YAG), it can be assumed that the gain seen by a pulse travelling through the amplifier remains approximately constant in time and is given by (Yariv, 1976)

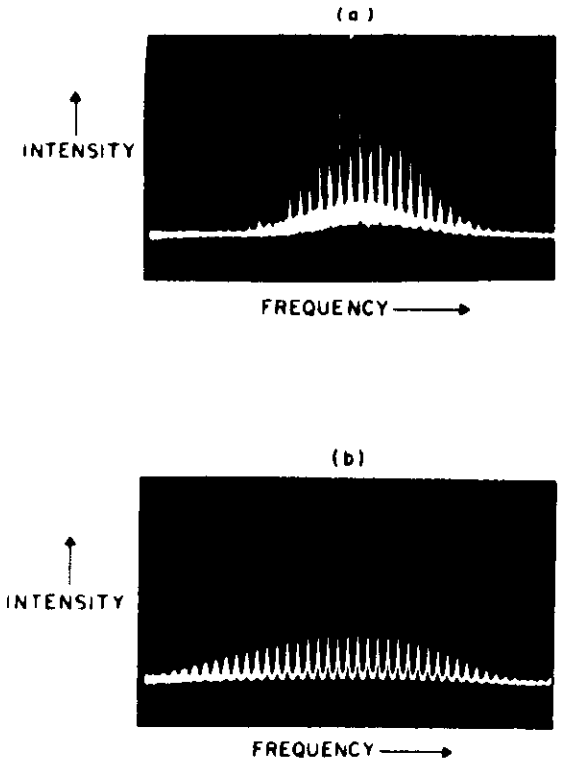

FIGURE 1.6 Frequency spectrum of (a) an unmodelocked laser and (b) the same laser after modelocking (Smith et al., 1975).

$$G = G_o(1 + I/I_s)^{-1} \tag{1.5}$$

where I is the average internal intensity and I_s is the saturation intensity. The loss consists of two terms, a constant L and a time varying modulation $L_m(1 - \cos \omega_m t)$, which can act to shorten the pulse with each roundtrip. Pulse spreading is produced by the frequency dependence (i.e. bandwidth limitation) of the gain. If the gain profile is approximated to be parabolic in frequency about line center: $1 - [(\omega - \omega_o)/\omega_G]^2$ then its effect in the time domain can be represented by its Fourier transform equivalent: a term proportional to the second

derivative of the pulse profile (Haus, 1975a; Haus, 1982). A small mismatch between modulation frequency and cavity roundtrip time, can be accounted for by addition of a term proportional to the first derivative of the pulse. One then has a differential equation for the steady state pulse amplitude (envelope) (Haus, 1982):

$$\{G - L - L_m(1 - \cos \omega_m t)\} E(t) = - \left\{\delta T_R \frac{d}{dt} + \frac{G}{\omega_G^2} \frac{d^2}{dt^2}\right\} E(t) \tag{1.6}$$

where δT_R is the detuning parameter and ω_G is the bandwidth of the gain. This is a Mathieu equation (Abramowitz and Stegun, 1972) which yields solutions periodic at ω_m. Further simplification is achieved by letting $\delta T_R = 0$ and by approximating $\cos \omega_m t$ by $1 - (\omega_m t)^2/2$. Equation (1.6) then becomes the Schroedinger equation for a particle in a parabolic potential. Its solutions are known to be of the form

$$E(t) = H_n(\omega_p t) \exp\left\{\frac{-\omega_p^2 t^2}{2}\right\} \tag{1.7}$$

where H_n is the Hermite polynomial of order n and

$$\omega_p = (\omega_m \omega_g)^{1/2} (L_m/2G)^{1/4}. \tag{1.8}$$

The full width at half maximum intensity of the lowest order pulse is

$$t_p = (2 \ln 2)^{1/2}/\omega_p. \tag{1.9}$$

It can be shown (Haus, 1975a) that gain saturation favors the lowest order mode and causes the higher order modes to be unstable in the steady state. So, pulses obtained by active modelocking of homogeneously broadened lasers with low emission cross-sections are Gaussian in shape and have a pulse duration that is inversely proportional to the square root of the gain bandwidth. These features of the theory have been verified experimentally with Nd:YAG

lasers (Kuizenga and Siegman, 1970b) and with high-pressure CO_2 systems (Smith et al., 1972). One word of caution is in order regarding the above analysis. In high gain laser systems such as dyes, F-centers and semiconductors gain saturation during the pulse is appreciable and the gain cannot be assumed constant. This dynamic saturation and recovery between pulses can then lead to a shorter pulse than that predicted by (1.6).

1.4 Passive Modelocking with a Fast Saturable Absorber

The shortest pulses have been produced by passive modelocking, first demonstrated with the ruby laser (Mocker and Collins, 1965) and the Nd:glass laser (DeMaria et al., 1966) and since utilized in virtually every type of laser (Smith et al., 1975). Results obtained with passive modelocking vary considerably from system to system, depending upon the medium response times as well as gain and absorber cross-sections. It is convenient for purposes of analysis to separate saturable absorbers into two classes: fast (or hard) and slow (or soft). A fast saturable absorber is one that recovers on a time scale shorter than the pulse duration so that it represents a loss given by

$$L_A = L_o \left(1 + \frac{I(t)}{I_{SA}}\right)^{-1} \tag{1.10}$$

where I_{SA} is the saturation intensity of the absorber and L_o is the small signal loss. In a dye, $L_o = \sigma_A N \ell$ where σ_A is the absorber cross-section, N is the concentration and ℓ is the path length. The saturation intensity is $\hbar\omega_o/\sigma_A\tau$ where τ is the dye absorption recovery time.

The steady state theory of fast absorber modelocking can be discussed in terms of an electronic regenerative pulse generator (Cutler, 1955). With a nonlinear element, called an expandor, in the feedback loop, Cutler showed that such a generator produced pulses with separation equal to the group delay of one roundtrip

and with a duration inversely proportional to the bandwidth. Cutler's analysis even provided expressions for pulse duration in the presence of group velocity dispersion in the loop.

If we expand the saturable loss to first order in $I(t) = |E(t)|^2$ such that

$$L_A \approx L_o \left(1 - \frac{|E(t)|^2}{I_{SA}}\right) \tag{1.11}$$

we can again write a differential equation for the steady pulse envelope (Haus, 1975b):

$$(G - L)\, E(t) = -\left\{\frac{G}{\omega_G^2}\frac{d^2}{dt^2} + \frac{L_o|E(t)|^2}{I_{SA}}\right\} E(t) \tag{1.12}$$

for which the gain, loss, and bandwidth limiting terms have the same meaning as in the previous section on active modelocking. Here again we note that the gain plays no dynamic role in pulse shaping. All of the self-narrowing comes from the instantaneously responding saturable absorption term. This self-narrowing achieves a balance with the spreading due to limited gain bandwidth. The solution is

$$E(t) = E_o\, \mathrm{sech}(t/t_p) \tag{1.13}$$

where

$$t_p = \frac{1}{\omega_G}\left\{\frac{2GI_{SA}}{L_o|E_o|^2}\right\}^{1/2} \tag{1.14}$$

and

$$L - G = \frac{G}{\omega_G^2 t_p^2}\,. \tag{1.15}$$

Several features are worth mentioning. The pulsewidth is now inversely proportional to the bandwidth, and the wings of the pulses

are exponential rather than the Gaussian characteristic of active modelocking.

Comparison of experiment with theory in this case is somewhat more difficult. Lasers for which fast saturable absorber modelocking is important (i.e. Nd:glass and Nd:YAG) tend to be operated in a transient rather than steady state regime. By the time steady state is reached, pulses in the laser can be so intense that nonlinear effects give rise to spectral broadening and pulse distortion (von der Linde, 1972; Duguay et al., 1970; Korobkin et al., 1970). For most scientific applications, therefore, single pulses are selected from the pulse train during transient build-up (von der Linde, 1972; Zinth et al., 1977). The selection and evolution of picosecond pulses from noise fluctuations has been analyzed in considerable detail theoretically and numerically (Fleck, 1970; Kryukov and Letokhov, 1972; New, 1979). Various experimental studies with different systems have found pulses approximately $\mathrm{sech}(t/t_p)$ in shape (Auston, 1971), pulses with Gaussian leading edges but exponential tails (von der Linde, 1972) and well-defined Gaussian pulses (von der Linde and Laubereau, 1971). One final, practical point is that the saturable absorbers used in these lasers are only "fast" in a relative sense. In fact, they have recovery times in the range 8-9 psec (von der Linde and Rodgers, 1973) which may work well to select pulses but which is not shorter than the pulses in most cases. This will certainly introduce some asymmetry into the shaping process.

1.5 Passive Modelocking with a Slow Saturable Absorber

Studies of passively modelocked flashlamp-pumped dye lasers (Arthurs et al., 1973a, 1973b; Dempster et al., 1972) revealed that the saturable absorber recovery times in these lasers were in the range 100 psec to 1 nsec, much longer than the duration of the pulses being generated. An insightful rate equation analysis by New (1974) then confirmed that the combined action

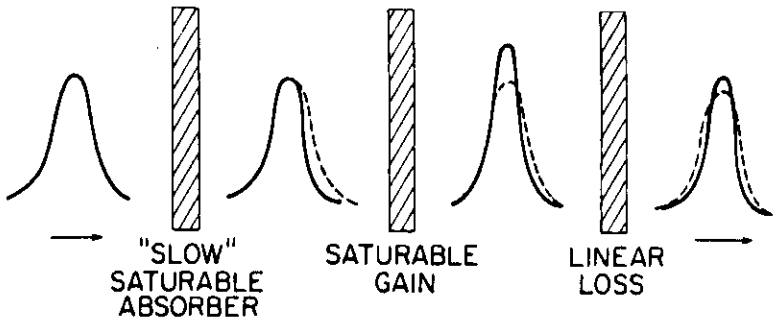

FIGURE 1.7 Transmission of a pulse through a slow saturable absorber, saturable amplifier, and linear loss can result in pulse shortening.

of gain saturation and absorber saturation could generate ultrashort pulses even in the absence of a fast recovery time. The idea is illustrated in Figure 1.7. As the pulse passes through the slow absorber, its front edge is absorbed more strongly than the peak and the trailing edge. The absorber simply becomes increasingly more transmissive with time since its recovery time is longer than the pulse duration. A simple dye rate equation in this limit yields:

$$L(t) = L_o \exp\left\{-\frac{\sigma_A}{\hbar\omega_o}\int_{-\infty}^{t} |E(t)|^2\, dt\right\} \qquad (1.16)$$

where $|E(t)|^2$ is again the optical intensity in watts/cm^2, $\hbar\omega_o$ is the photon energy, σ_A is the absorber cross-section, and $L_o = \sigma_A N \ell$ is the small signal absorption.

When the pulse passes through the gain medium it receives less amplification in the trailing edge because of gain saturation. The gain, which also recovers slowly on the time scale

of the pulse, is given by

$$G(t) = G_o \exp\left\{-\frac{\sigma_G}{\hbar\omega_o}\int_{-\infty}^{t} |E(t)|^2\, dt\right\} . \qquad (1.17)$$

Finally, the other (D.C.) losses of the system reduce, in the steady state, the pulse energy to its initial value. To complete the cycle, both gain and absorber elements recover substantially but not completely before the pulse returns. Within certain ranges of round trip time and under the basic condition

$$\sigma_A > \sigma_G \qquad (1.18)$$

it can be shown (New, 1974; Haus, 1975c) that a pulse of constant (steady state) energy can be progressively shortened with each round trip. Although an excess of gain is needed to start pulse build-up, in the steady state the absorption is at a higher value than the gain until arrival of the pulse. The greater saturability of the absorber results in the peak of the pulse receiving net gain; then gain saturation leads to net loss for the trailing edge. Figure 1.8 illustrates this behavior as a function of time.

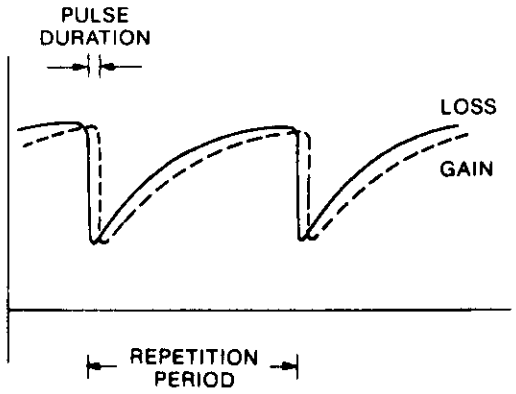

FIGURE 1.8 Steady state dynamics of a laser modelocked by a slow saturable absorber. Note that the gain recovers less rapidly than the loss so that the leading edge of the pulse experiences loss.

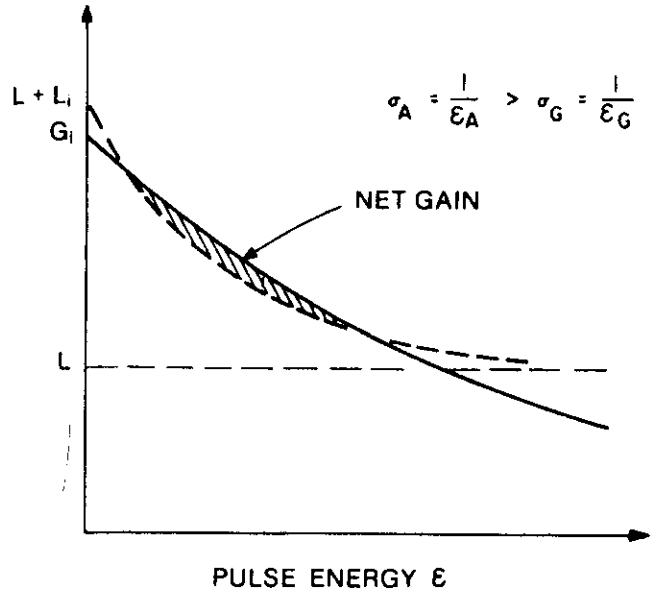

FIGURE 1.9 Gain and loss as a function of pulse energy.

Figure 1.9 illustrates the saturation of both gain and loss according to (1.16) and (1.17) and the inequality of (1.18). The integrated pulse energy ε advances in time from zero, where there is net loss, through the region of net gain to the end of the pulse where the gain is again less than the loss. In (1.16) and (1.17) we have used the same pulse intensity $|E(t)|^2$. In practice it is common to focus more tightly in the saturable absorber. In our notation this can be accounted for by an "effective" σ_A which is increased relative to σ_G by the inverse ratio of the beam areas.

With certain approximations we can again write a differential equation for this case (Haus, 1975c; Haus, 1982):

$$\{G(t) - L(t) - 1\}\, E(t) = -\left\{\frac{L}{\omega_G^2}\frac{d^2}{dt^2} + \frac{\delta}{\omega_G}\frac{d}{dt}\right\} E(t) \qquad (1.19)$$

where the gain $G(t)$ and the loss $L(t)$ have the dependence on pulse energy discussed above. A detuning term (proportional to

d/dt) must be added here to facilitate a solution. Remember that for active modelocking and for modelocking with a fast absorber it was possible to find a solution with zero detuning, but that is not the case here. To obtain an analytical solution we expand (1.16) and (1.17) to second order in pulse energy

$$G(t) = G_i \left\{1 - \sigma_G \varepsilon(t) + \frac{\sigma_G^2 \varepsilon^2}{2}(t)\right\} \tag{1.20}$$

and

$$L(t) = L_i \left\{1 - \sigma_A \varepsilon(t) + \frac{\sigma_A^2 \varepsilon^2}{2}(t)\right\} \tag{1.21}$$

where

$$\varepsilon(t) = \frac{1}{\hbar\omega_0} \int_{-\infty}^{t} |E(t)|^2 \, dt \tag{1.22}$$

and G_i and L_i are the "initial" values of gain and loss just prior to pulse arrival. Both G_i and L_i depend upon recovery times and cavity round-trip time.

The solution of (1.19) is

$$E(t) = E_0 \operatorname{sech}(t/t_p) \tag{1.23}$$

where

$$t_p = \frac{4}{\omega_G} \left(\frac{1}{\sigma_A \varepsilon_\infty}\right) (L/L_i)^{1/2}. \tag{1.24}$$

Here ε_∞ is the total pulse energy (i.e. $t \to \infty$ in (1.22)) and L/L_i is the ratio of D.C. loss to saturable absorber loss. The pulsewidth is again proportional to the inverse of the resonator bandwidth which we have called the gain bandwidth. If the solution (1.23) is plugged back into (1.19), one gets, in addition to (1.24), two other characteristic equations for the pulse

amplitude E_0 and the detuning parameter δ.

This analysis by Haus (1975c) provided the first closed form solutions of pulse shape and the first predictions of pulse duration in the presence of bandwidth limitation. Although several approximations are made, namely parabolicity of the frequency restriction and second-order expansion of loss and gain, the results obtained from this theory have been found to be surprisingly accurate when compared with more involved numerical calculations (Hermann et al., 1981; Hermann and Weidner, 1982; Stix and Ippen, 1982).

With successful operation recently of the passively modelocked dye laser in a bidirectional (CPM) ring configuration (Fork et al., 1981), some interest has been focused on the effect of coherent pulse coupling and interation in the saturable absorber. The modelocking dynamics of this system are similar in many respects to those of conventional slow absorber modelocking. Important differences are: (a) pulses traveling in opposite directions pass through the absorber at the same time (if the absorber is thinner than the pulses) but through the gain medium at different, well-separated times; and (b) the colliding pulses in the absorber interfere to form an absorption grating which in turn coherently scatters light from each pulse into the other. The first condition results in an effective increase in the ratio of absorber cross section σ_A to gain cross section σ_B by a factor of 2. This provides increased stability and can help generate shorter pulses. The coherent coupling interaction (b) can be included in the analysis numerically (Hermann et al., 1981; Stix and Ippen, 1982). The bleaching and generation of an absorption grating as a function of time in the thin absorber are illustrated in Figure 1.10. Pulse shaping due to these dynamics are given in Figure 1.11 for a single pass through the absorber. The dash-dot line is the shape of the input pulse; the dashed shape would be the transmitted shape of one of the pulses if it passed through the absorber by itself; the dotted line is also for a single pulse,

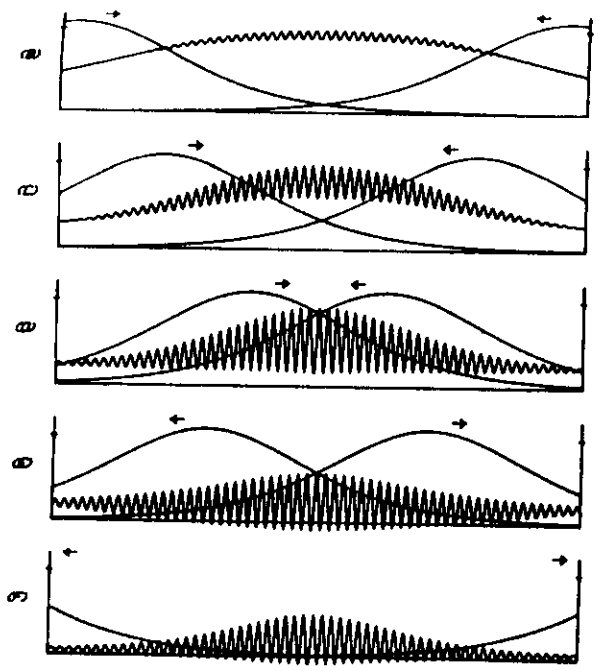

FIGURE 1.10 Pulses incident from opposite ends interface and create an absorption grating. Time sequence from top to bottom.

but focused to one-third the area; and the solid line is the actual result obtained with colliding pulses and inclusion of the grating effect. Surprisingly, the complication introduced by coherent coupling can very closely be mimicked by tighter focusing (or by an increase in the absorber cross-section). The enhancement due to the coupling is a factor of 1.5, so that the overall enhancement in CPM is the factor of three. Although Figure 1.11 shows only one pass through the saturable absorber, similar results have been obtained for steady state pulses in a system with saturable loss; saturable gain, and dispersion. As the pulses begin to get shorter than the thickness of the absorber, the cross-section enhancement factor, and hence the pulse

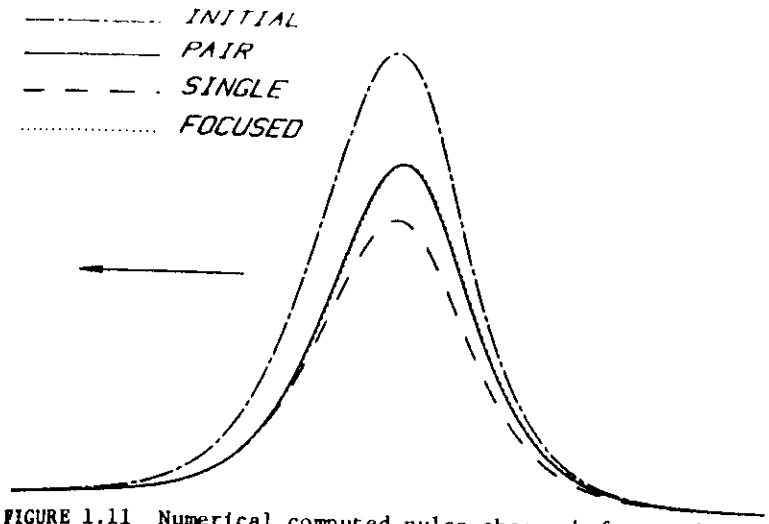

FIGURE 1.11 Numerical computed pulse shapes before and after passage through a slow saturable absorber (see text).

shortening velocity, begins to decrease, but pulses do continue to get shorter until a balance is struck with the dispersion of the resonator. At the current, femtosecond, state-of-the-art, small amounts of dispersion in dye streams and in mirror coatings become increasingly problematic. Schemes for generating shorter pulses will most likely involve clever, dispersion-compensating design of these passive elements. An alternative approach is the nonlinear optical compression described below.

1.6 Ultrashort Pulse Propagation

In the previous sections we discussed ultrashort pulse generation by nonlinearly absorbing and amplifying elements. Now we turn to the propagation of such ultrashort pulses through essentially transparent media of also essentially unlimited bandwidth (in the spectral amplitude sense we have used above). In such media, and optical fibers are good examples, the primary forces of pulse distortion are group velocity dispersion and nonlinear phase changes. We now write the wave equation for the

electric field amplitude in the form (Whitham, 1974; Haus, 1982)

$$\frac{\partial E}{\partial z} + \frac{1}{v_g}\frac{\partial E}{\partial t} = \frac{i}{2}\frac{\partial^2 \beta}{\partial \omega^2}\frac{\partial^2 E}{\partial t^2} - \frac{i\pi}{\lambda n} n_2 |E|^2 E. \qquad (1.25)$$

The left hand side of this equation describes free propagation of the pulse with the group velocity $v_g = (\partial\beta/\partial\omega)^{-1}$. The usual, slowly-varying-envelope approximation has been assumed. On the right hand side of the equation, the first term is a diffusion term arising from variation of the group velocity with frequency; the second term can be thought of either as a nonlinear velocity term or as a nonlinear (self-phase modulation) driving polarization. With a rather simple transformation, (1.25) reduces to the nonlinear Schroedinger equation (Mollenauer et al., 1980; Nakatsuka et al., 1981; Haus, 1982).

Let us first consider the distorting terms separately. After propagation over a long distance a pulse will spread out due to group velocity dispersion with (for normal dispersion $\partial^2\beta/\partial\omega^2 < 0$) the high frequencies trailing the lower frequencies. It can be shown (Unger, 1977; Marcuse, 1980) that a coherent Gaussian pulse of duration (full 1/e intensity width) τ will broaden to a width

$$\tau' = \tau\sqrt{1 + (\tau_c/\tau)^4} \qquad (1.26)$$

where the "critical" pulsewidth is

$$\tau_c = (2)^{5/4}\sqrt{L\frac{\partial^2\beta}{\partial\omega^2}}$$

for a propagation length L. Clearly pulses shorter than τ_c spread rapidly.

If a pulse is dispersed in the above manner, no spectral amplitudes have been changed and the pulse can be reconstructed by transmission through an equivalent length of opposite dispersion, as has been suggested for optical fiber systems (Marcuse and Lin,

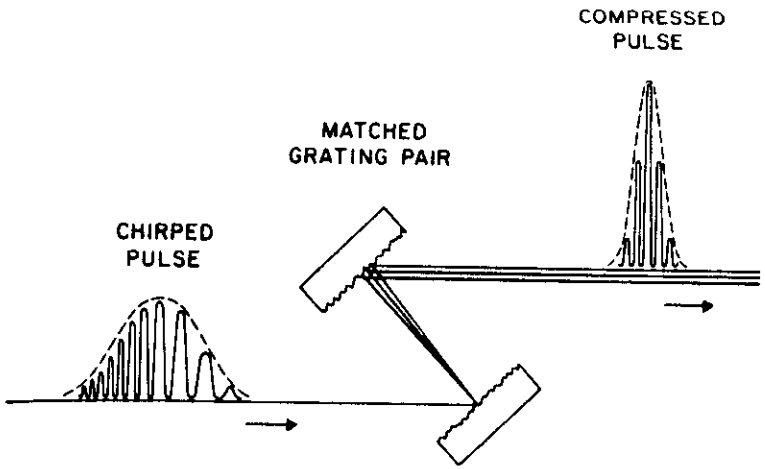

FIGURE 1.12 Compression of a chirped pulse by a matched pair of gratings (Treacy, 1969).

1981). A laboratory technique for this recompression of a chirped pulse is shown in Figure 1.12 (Treacy, 1969). The grating pair technique is versatile because the degree of anomalous dispersion is easily variable by changing the distance L between the gratings

$$L\frac{\partial^2\beta}{\partial\omega^2} = \frac{L\lambda^3}{2\pi c^2 d^2\,(1 - (\lambda d - \sin\gamma)^2)} \qquad (1.28)$$

where d is the number of lines/cm on the grating and γ is the angle between the incident light and the grating normal. Recompression has also recently been demonstrated in sodium vapor (Nakatsuka et al., 1981) and with excitonic dispersion in GaAs (Fehrenbach and Salour, 1982).

Through the self-phase modulation term on the right hand side of (1.25) a pulse can cause a rapid modulation of its own phase and hence a frequency upshift on the rise and a downshift in the trailing half. Since the pulse shape is not changed by this action, anamolous dispersion, such as that provided by a grating pair, may then be used to compress the pulse (Laubereau,

1969; Lehmberg and McMahon, 1976). Pulse compression is limited in general because the frequency chirp is not linear over the entire pulse.

The advantage optical fibers presented for enhancing self-phase modulation was recognized early (Ippen et al., 1974; Stolen and Lin, 1978) and interesting pulse shaping effects that occurred in the presence of dispersion were pointed out (Fisher and Bischel, 1975). More recently, it was realized (Grischkowsky and Balant, 1982) that the proper combination of fiber dispersion and self-phase modulation could produce a more uniform chirp over the entire pulse length. This principle then led (Shank et al., 1982) to the compression of pulses to 30 fsec with a 15 cm fiber and a grating pair.

A number of years ago it was also pointed out (Hasegawa and Tappert, 1973) that the self-phase modulation term could be used to compensate for the pulse broadening effect of dispersion. In the simplest case, with the proper sign of dispersion and with a $\mathrm{sech}(t/t_p)$ pulse envelope, the two terms on the right hand side of (1.25) can cancel. The pulse then propagates distortion free as a 'soliton'. Higher order soliton solutions that are periodic in their propagation characteristics are also possible (Zakharov and Shabat, 1973; Satsuma and Yajima, 1974). With the advent of picosecond laser sources (Mollenauer and Bloom, 1979) in the wavelength regime of negative group velocity dispersion ($\sim$ 1.55 μm), experimental demonstration of soliton formation and propagation was made possible (Mollenauer et al., 1980). In addition to opening up the possibility of interesting, scientific studies of soliton behavior, this work may point the way to eventual, practical control of ultrashort pulse propagation in optical fibers.

REFERENCES

Abramowitz, H., and I.A. Stegun, eds., 1972, *Handbook of Mathematical Functions* (Dover, New York).

Alfano, R.R., and S.L. Shapiro, 1971, Chem. Phys. Lett. 3, 407.

Arthurs, E.G., D.J. Bradley, and A.G. Roddie, 1973a, Chem. Phys. Lett. 22, 230.

Arthurs, E.G., D.J. Bradley, and A.G. Roddie, 1973b, Appl. Phys. Lett. 23, 88.

Auston, D.H., 1971, Appl. Phys. Lett. 18, 249.

Bloom, D.M., L.F. Mollenauer, C. Lin, D.W. Taylor, and A.M. DelGaudio, 1979, Opt. Lett. 4, 297.

Bradley, D.J., 1977, *Ultrasound Light Pulses*, Topics in Appl. Phys. 18, edited by S.L. Shapiro (Springer Verlag).

Cohen, L.G., and C. Lin, 1977, Appl. Opt. 16, 3136.

Cutler, C.C., 1955, Proc. I.R.E. 43, 140.

DeMaria, A.J., D.A. Stetser, and H. Heyman, 1966, Appl. Phys. Lett. 8, 22.

Dempster, D.N., T. Morrow, R. Rankin, and G.F. Thompson, 1972, J. Chem. Soc. Faraday II 68, 1479.

Edgerton, H.E., 1932, J. SMPTE 18, 356.

Fehrenbach, G.W., and M.M. Salour, 1982, *Picosecond Phenomena III* (Springer-Verlag).

Fisher, R.A., and W.K. Bischel, 1975, J. Appl. Phys. 46, 4921.

Fork, R.L., B.I. Greene, and C.V. Shank, 1981, Appl. Phys. Lett. 38, 671.

Grischkowsky, D., and A.C. Balant, 1982, Appl. Phys. Lett.

Haus, H.A., 1975a, IEEE J. Quant. Electron. QE-11, 323.

Haus, H.A., 1975b, J. Appl. Phys. 46, 3049.

Haus, H.A., 1975c, IEEE J. Quant. Electron. QE-11, 736.

Haus, H.A., 1982, *Waves and Fields in Optoelectronics* (Prentice Hall).

Hermann, J., and F. Weidner, 1982, to be published.

Hermann, J., F. Weidner, and B. Wilhelmi, 1981, Appl. Phys. B 26, 147.

Ippen, E.P., and C.V. Shank, 1975a, Appl. Phys. Lett. 27, 488.

Ippen, E.P., C.V. Shank, and A. Dienes, 1972, Appl. Phys. Lett. 21, 348.

Ippen, E.P., C.V. Shank, and T.K. Gustafson, 1974, Appl. Phys. Lett. 24, 190.

Jang, S.J., L.G. Cohen, W.L. Mammel, and M.A. Saifi, 1982, B.S.T.J. 61, 385.

Korobkin, V.A., A.A. Malyutin, and A.M. Prokhorov, 1970, JETP Lett. 12, 150.

Kuizenga, D.J., and A.E. Siegman, 1970a, IEEE J. Quant. Electron. QE-6, 694.

Kuizenga, D.J., and A.E. Siegman, 1970b, IEEE J. Quant. Electron. QE-6, 709.

Kryukov, P.F., and V.S. Letokhov, 1972, IEEE J. Quant. Electron. QE-8, 766.

Laubereau, A., 1969, Phys. Lett. 29A, 539.

Lehmberg, R.H., and J.M. McMahon, 1976, Appl. Phys. Lett. 28, 204.

Li, T., 1978, IEEE Trans. Commun. 26, 946.

Lin, C., L.G. Cohen, W.G. French, and V.A. Foertmeyer, 1978, Electron. Lett. 14, 170.

Marcuse, D., 1980, Appl. Opt. 19, 1653.

Marcuse, D., and C. Lin, 1981, IEEE J. Quant. Electron. QE-17, 869.

Mija, T., Y. Terunuma, T. Hosaka, and T. Miyashita, 1979, Electron. Lett. 15, 106.

Mija, T., K. Okamoto, Y. Ohmori, and Y. Sasaki, 1981, IEEE J. Quant. Electron. QE-17, 858.

Mocker, H.W., and R.J. Collins, 1965, Appl. Phys. Lett. 7, 270.

Mollenauer, L.F., R.H. Stolen, and J.P. Gordon, 1980, Phys. Rev. Lett. 45, 1095.

Nakatsuka, H., D. Grishkowsky, and A.C. Balant, 1981, Phys. Rev. Lett. 47, 910.

New, G.H.C., 1974, IEEE J. Quant. Electron. QE-10, 115.

New, G.H.C., 1979, Proc. IEEE 67, 380.

Porter, G., 1950, Proc. Roy. Soc. (London) A200, 284.

Satsuma, J., and N. Yajima, 1974, Supp. Prog. Theor. Phys. 55, 284.

Schmidt, W., and F.P. Schäfer, 1968, Phys. Lett. 26A, 558.

Shank, C.V., and E.P. Ippen, 1974, Appl. Phys. Lett. 24, 373.

Shank, C.V., R.L. Fork, R. Yen, R.H. Stolen, and W.J. Tomlinson, 1982, Appl. Phys. Lett. 40, 761.

Shapiro, S.L., 1977, *Ultrashort Light Pulses*, Topics in Appl. Phys. 18, edited by S.L. Shapiro (Springer Verlag), 1-15.

Smith, P.W., M.A. Duguay, and E.P. Ippen, 1975, Prog. in Quant. Electron., edited by Sanders and Stenholm (Pergamon Press), 8, 107-229.

Stix, M., and E.P. Ippen, 1982, to be published.

Stolen, R.H., and C. Lin, 1978, Phys. Rev. A17, 1448.

Treacy, E.B., 1969, IEEE J. Quant. Electron. QE-5, 454.

Unger, H.G., 1977, Arch. Elec. Ubertragung 31, 518.

von der Linde, D., 1972, IEEE J. Quant. Electron. QE-8, 328.

von der Linde, D., and A. Laubereau, 1971, Opt. Commun. 3, 27.

von der Linde, D., and K.F. Rodgers, 1973, IEEE J. Quant. Electron. QE-9, 960.

von der Linde, D., O. Bernecker, and A. Laubereau, 1970, Opt. Commun. 2, 215.

Whitham, G.B., 1974, *Linear and Nonlinear Waves* (John Wiley and Sons, New York).

Yariv, A., 1976, *Introduction to Optical Electronics* (Holt, Rinehart, Winston).

Zakharov, V.E., and A.B. Shabat, 1973, Sov. Phys. JETP 37, 823.

Zinth, W., A. Laubereau, and W. Kaiser, 1977, Opt. Commun. 22, 161.

2. PICOSECOND AND SUBPICOSECOND LASER SYSTEMS

2.1 Introduction

Although the first picosecond pulses were generated more than fifteen years ago (DeMaria et al., 1966), we are now witnessing a rapidly increasing interest in ultra-short pulse techniques and their application to dynamic studies. This is largely due to the emergence of new laser systems that offer broader wavelength coverage, sub-picosecond resolution, more sensitivity, high repetition rates, and greater reliability. Figure 2.1 compares, in two dimensions at least, several of the most important ultrashort pulse laser systems currently available. The dots indicate the primary oscillating wavelengths and easily generated harmonics of the Nd:glass and cw passively-modelocked Rhodamine 6G systems. Connecting lines indicate that all intermediate wavelengths have been generated by nonlinear optical, frequency conversion techniques. As indicated by the bars, synchronously-pumped dye lasers and color center lasers offer continuously tunable cw pulse trains, albeit not with a single pumping source or gain medium. It should

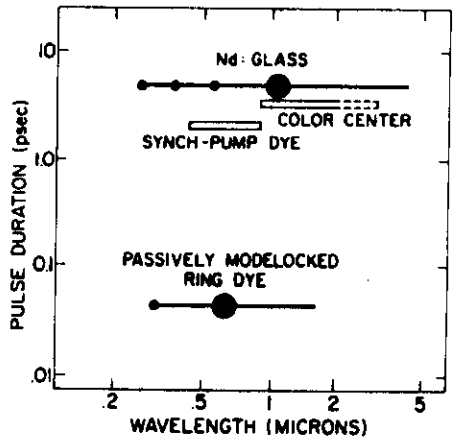

FIGURE 2.1 Wavelength coverage and typical pulse durations of available ultrashort pulse lasers.

be noted that specific experimental considerations influence the choice of system for a particular application; pulse duration may not be the only factor determining temporal resolution in each case. Nevertheless, the passively-modelocked cw dye laser has a clear advantage in this regard. It is also a high repetition rate system that can take advantage of powerful signal averaging techniques.

In this chapter we review and discuss some of the characteristics of the systems indicated in Figure 2.1.

2.2 Nd:Glass Laser

Over the years the pulse output characteristics of this laser have perhaps been the most extensively investigated (Shapiro, 1977). These investigations have to a certain extent been necessitated by the variety and variability of pulse outputs obtained. Pulse characteristics vary greatly with differences in laser design, from shot to shot in a particular system, and with position in the train of pulses produced by a single flash. Much of this behavior can be explained in terms of transient laser build-up from an initially statistical distribution of fluctuations (Kryukov and Letokhov, 1972). Selection of a single, short, isolated pulse under these conditions requires careful control of a variety of parameters. It is especially important that the laser be operated in a low order transverse mode, near threshold, and that spurious reflections and beam irregularities be avoided. In order to avoid satellite pulses the saturable absorber is generally placed in direct contact with one of the end mirrors of the laser (Bradley et al., 1970). A fast (picosecond recovery time) saturable absorber is required. An interesting alternative to using a contacted dye cell involves the use of the anti-resonant ring (Siegman, 1973) shown in Figure 2.2. With a 50% beamsplitter, the antiresonant ring has the property that all of the incident light is reflected back along the incoming path. Pulses traveling in opposite di-

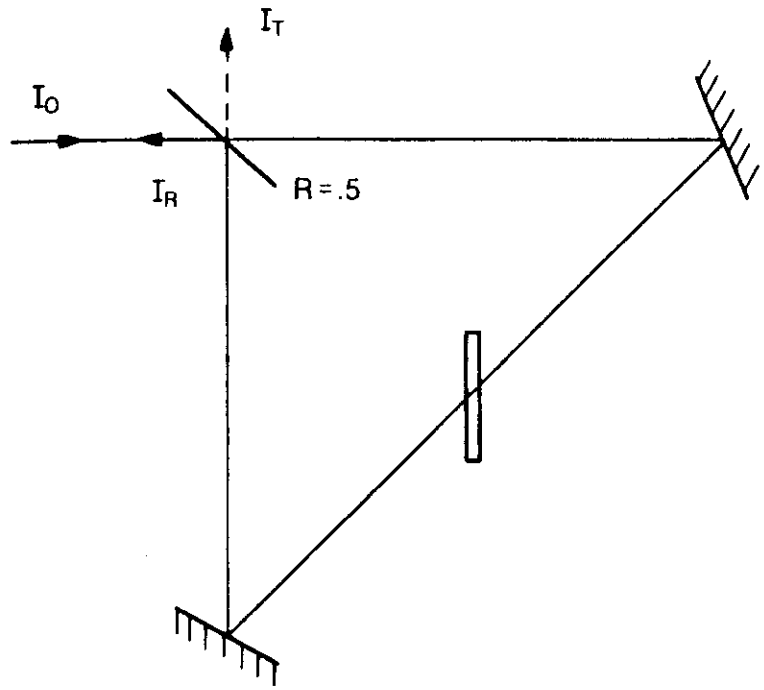

FIGURE 2.2 An antiresonant ring configuration for effective saturable absorber modelocking

rections around the ring always have the same path lengths and exactly cancel in the transmission direction. A saturable absorber positioned where the counterpropagating pulses collide is effectively at the end of the resonator. It can be inserted at Brewster's angle to reduce the usual etalon effects of a contacted dye cell. Pulsewidth reduction from 30 psec to 15 psec in a passively modelocked Nd:YAG laser has recently been obtained with this scheme (Vanherzeele and Siegman, 1982).

The build-up of Nd:glass laser pulse trains and the variation of pulse characteristics during this build-up have been studied by many workers (Shapiro, 1977). During the first part of the flashlamp pumping, spontaneous emission fluctuations are

amplified linearly. When they reach sufficient intensity to begin bleaching the saturable absorber, the largest fluctuation peak grows most rapidly and takes over. Although gain saturation plays a role in emphasizing the largest peak (Glenn, 1975) it probably does not have a dramatic effect on pulse shape. (This is in direct contrast to dye lasers where strong gain depletion and gain recovery can occur within a cavity round-trip time.) As the main intensity peak (now a "mode-locked pulse") continues to grow in amplitude, nonlinearities of the glass laser medium (self-phase modulation and self-focusing) start to introduce new spectral broadening and temporal sub-structure (Duguay et al., 1970; Korobkin et al., 1970). If the gain is too high, the pulse can literally be torn apart (Eckhardt et al., 1974).

Because of this great variation between pulses within a train, accurate picosecond measurements must be made with single, properly selected, pulses (von der Linde, 1972; Zinth et al., 1977). Pulse selection is accomplished by passing the pulse train through a high speed Pockels cell or Kerr shutter that is activated by a high voltage spark gap (von der Linde et al., 1970). When the laser output reaches a predetermined level, the spark gap fires and the next pulse is transmitted. Usually the pulse is chosen to be near the beginning of the train (as viewed on an oscilloscope). At this point the laser is already in the regime where the primary fluctuation peak has been isolated but subsequent broadening has not yet come strongly into play. In a carefully designed system it is possible, in this way, to obtain pulses with an average pulsewidth of about 5 psec and an rms width fluctuation of about 0.5 psec (Zinth et al., 1977). These pulses can be in a low order transverse mode and have energies of several millijoules. Thus peak powers are around 10^9 watts, already sufficient for efficiently driving a variety of nonlinear processes. In nonlinear experiments, however, the fluctuation of pulse characteristics becomes increasingly problematic. Care must be taken

to characterize each pulse used.

Some applications require even higher powers than can be obtained by a single Nd:glass oscillator. Just a few comments are in order here. Picosecond pulses saturate amplifier gain with pulse energy. In the case of Nd:glass, saturation energy density is about $5 J/cm^2$. This means that Nd:glass amplifiers can only be operated in a small-signal-gain, low efficiency configuration. Even with 5 psec pulses, operation near saturation would result in peak powers of 10^{12} watts/cm^2. At this point destructive nonlinear effects in the glass would be overwhelming. Although pulse energies of several joules can be achieved, such very high power systems are complicated, expensive, and are needed only for a very few applications such as very short wavelength generation (Reintjes et al., 1977; Attwood et al., 1977).

An area in which Nd:glass systems have been especially useful has been in the generation and utilization of picosecond infrared pulses (Kaiser et al., 1980; Kaiser and Laubereau, 1977). With 9400 cm^{-1} (1.06 μm) pulses it is possible to generate tunable infrared pulses between 2500 cm^{-1} and 7000 cm^{-1} by three-photon parametric mixing in $LiNbO_3$ (Laubereau et al., 1974). With two $LiNbO_3$ crystals, separated by about 50 cm, considerable reduction in divergence and bandwidth is achieved (Seilmeier et al., 1978). By addition of yet another stage, and by introducing appropriate delay between the pump and signal beam, pulse durations have reduced into the sub-picosecond regime (Fendt et al., 1979). Generation of broadband tunable picosecond pulses for spectroscopy in the 10 μm - 20 μm by difference frequency mixing in CdSe has also been reported (Campillo et al., 1979).

2.3 Synchronously Pumped CW Dye Lasers

The most common picosecond laser systems at this time are commercially available, synchronously pumped dye lasers. They offer tunable cw trains of picosecond pulses at wavelengths throughout the visible and into the near infrared. An actively

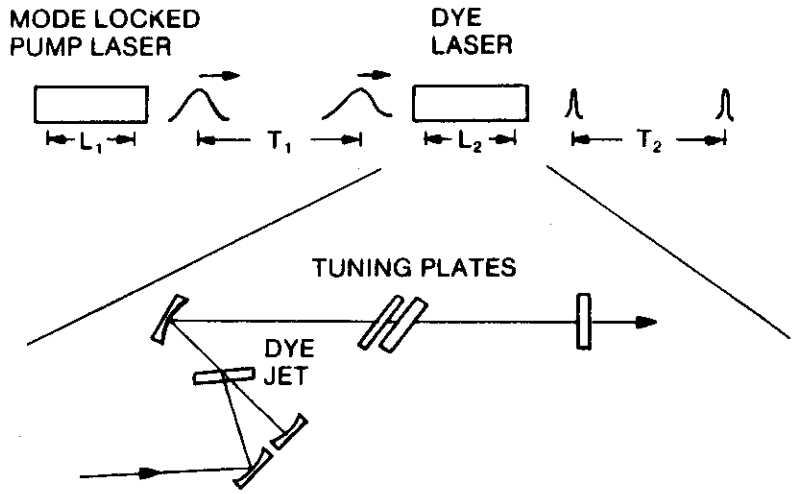

FIGURE 2.3 Schematic of a typical synchronously-pumped laser. The dye is contained in a free-flowing jet and birefringent plates provide tuning and bandwidth limitation.

modelocked pump laser (usually either an argon or krypton ion laser) is used to pump a cw dye laser of matching cavity length. A typical arrangement is shown in Figure 2.3. Pump pulses of about 100 psec in duration can be converted to dye laser pulses of several picosecond or less. The dye laser gain dynamics involved in this process are illustrated in Figure 2.4. Gain increases as the integral of the pump pulse until it exceeds the losses. The pulse within the dye laser then arrives and drives the gain below the loss line. Actual pulse-shapes are very critically dependent upon the round-trip time (hence arrival time) of the dye laser pulse (Ausschnitt and Jain, 1978). Sub-picosecond pulse durations are possible but very difficult to obtain in practice. Recent streak camera results (Shapiro et al., 1981) have shown pulse break-up and satellite pulse formation when

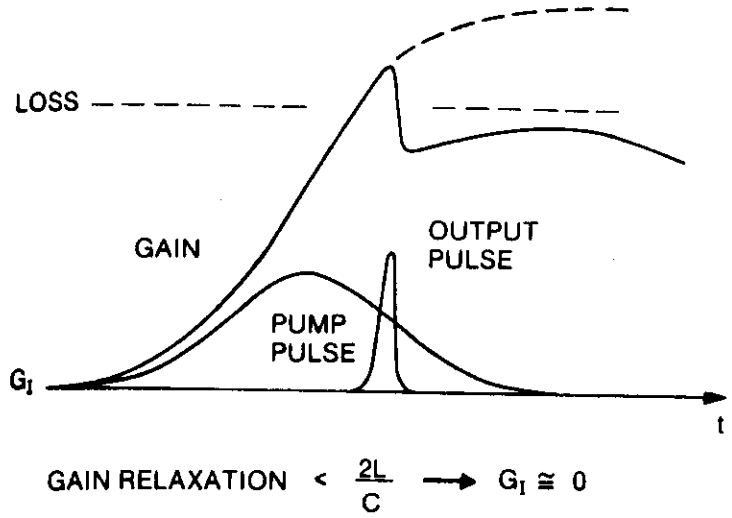

FIGURE 2.4 Gain dynamics as a synchronously-pumped dye laser.

ultrashort pulse operation is attempted. Satellite pulses form as the gain rises above the loss line for a second time. Some improvement in this regard may be achieved using a very small radius end mirror so that the gain jet is within several millimeters of the end of the resonator (Heritage et al., 1981). Then the dye laser pulse makes two passes through the gain in rapid succession.

Figure 2.5 indicates the broad spectral coverage provided by a relatively small number of dyes. Of increasing importance is the 800-900 nm region (Kuhl et al., 1977) of interest for time-resolved spectroscopy of GaAs and GaAlAs materials and structures. Dyes in this range have tended to be unstable and to require unpleasant solvents. Very recently, stable and efficient operation from 760 nm to 900 nm has been achieved with the single dye Oxazine 750 dissolved with propylene carbonate in ethylene glycol (Aumiller, 1982; Eilenberger et al.,

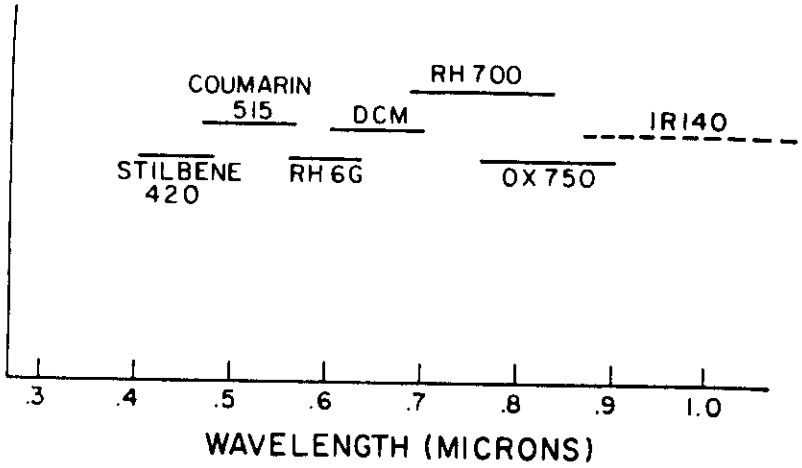

FIGURE 2.5 Efficient dyes for wavelengths spanning the visible and near infrared.

1982). Bandwidth limited pulses of about 5 psec in duration have been obtained over most of the range.

The ring geometry has been utilized by several groups for synchronous modelocking (Heritage and Isaacs, 1981; Halbout et al., 1981; Eilenberger et al., 1982), but the advantages of colliding pulse interaction here are still less clear than they are for passive modelocking.

Synchronous pumping also opens the possibility of operating two modelocked dye lasers simultaneously for experiments requiring pulses at two wavelengths. The two lasers can be operated in parallel (Heritage and Jain, 1978) pumped by the same argon laser, or in tandem (Jain and Heritage, 1975), where the first dye laser pumps the second. Most recently, a system providing two separately tunable, highly stable, cavity-dumped trains of 8 psec duration and low jitter has been developed (Heritage et al., 1982). Such a system will find many important applications in nonlinear, particularly Raman, spectroscopy (Heritage, 1980).

Although not yet in such wide usage as dye lasers, color center lasers offer many similar qualities, i.e. tunability and efficiency. Most importantly, they can provide cw picosecond pulse trains at wavelengths unreachable with dyes. An F_2^+ color center pumped by Nd:YAG and operating in the range 1.25 - 1.45 μm (Mollenauer and Bloom, 1979) made possible the first demonstration of long distance transmission of picosecond pulses in optical fibers (Bloom et al., 1979). Very recently, discovery of a new $T\ell^0(1)$ color center in KCℓ (Gellerman et al., 1981) has made possible (also with Nd:YAG pumping) the development of a picosecond source for the range 1.4 μm to 1.6 μm (Mollenauer et al., 1982). Both lasers are valuable diagnostic tools for this long wavelength regime. The new $T\ell^0(1)$ center in particular is stable at room temperature and, under laser excitation, free from orientational bleaching.

From a modelocking point of view the $T\ell^0(1)$ centers in KCℓ have interesting properties. In contrast to dyes they have a relatively low gain cross-section and a long (1600 nsec) radiative decay time. As a result, the shortest pulses are produced with synchronous pumping as far as possible above threshold in a high Q resonator (Mollenauer et al., 1982). The gain dynamics of such a system are illustrated in Figure 2.6. The long gain lifetime implies little relaxation in a round-trip time. Thus the gain prior to each pumping pulse is essentially clamped to its value following the previous lasing pulse. This has the important consequence of both stabilizing pulse energy and eliminating satellite pulses (Mollenauer et al., 1982; Haus, 1982b).

2.5 Passively Modelocked CW Dye Laser

The first sub-picosecond pulses were generated by the passively modelocked cw dye laser. A version of this laser that has

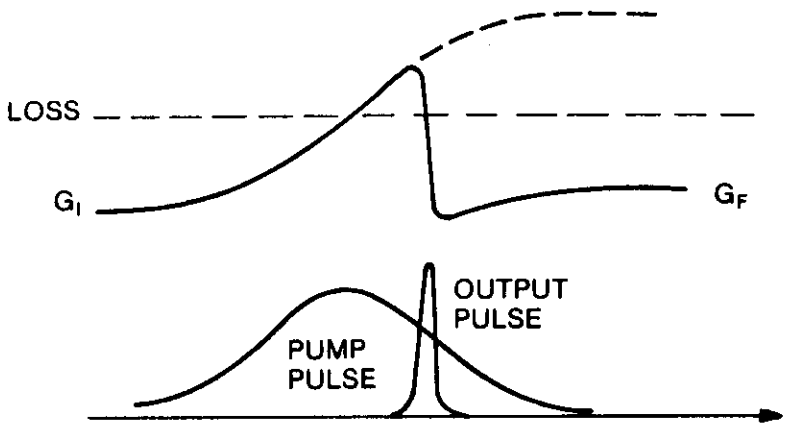

FIGURE 2.6 Gain dynamics in a synchronously pumped color center laser with a long gain lifetime.

been used successfully in a variety of picosecond studies is shown in Figure 2.7. The gain medium, rhodamine 6G in a free-

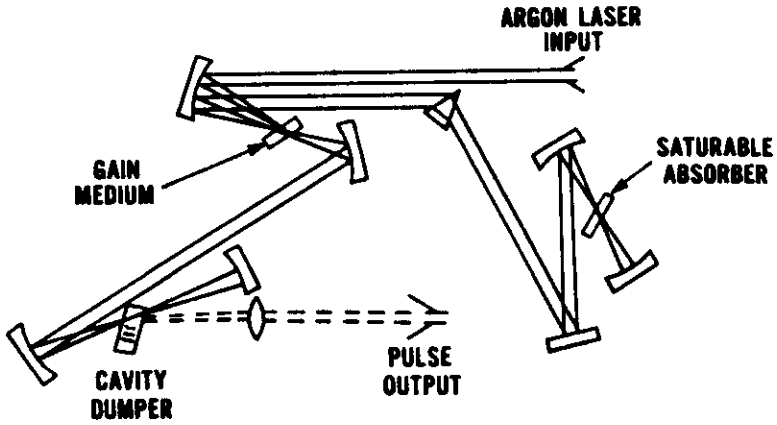

FIGURE 2.7. Cavity-dumped, passively modelocked cw dye laser.

flowing stream of ethylene glycol, is located at a focal point approximately in the center of the resonator. Near one end of the resonator is a second, free-flowing stream of ethylene glycol containing the saturable absorber dyes for modelocking. The beam waist in this stream is about a factor of two smaller than that in the gain medium. Sub-picosecond pulses can be generated with only the dye DODCI in the modelocking stream, but in this linear laser, addition of a second dye, malachite green, improves reproducibility and stability (Ippen and Shank, 1975a). The recovery time of DODCI in this system has been measured to be 1.2 nsec (Shank and Ippen, 1975), confirming its behavior as a "slow" absorber. Malachite green provides some absorption recovery on a picosecond time scale (Ippen et al., 1976) discriminating against satellites and facilitating sub-picosecond pulse operation in a stable regime well above threshold.

At the other end of the resonator is a commercially available cavity dumper that can dump single pulses from the laser at a rate of more than 10^5 pps. This arrangement is often preferable to taking the pulse output through a partially transmitting mirror. The peak power is at least an order of magnitude greater, and the lower repetition rate can be adjusted to allow for complete sample recovery (or replacement) between pulses.

The output pulses of the system shown in Figure 2.7 have been well characterized. Sub-picosecond pulses are generated near 615 nm. Energy in each pulse is about 5×10^{-9} J and the peak power exceeds 5 kW. In a focused beam, energy densities of several millijoules per square centimeter are easily achieved. When the highest temporal resolution is required, pulses can be compressed and filtered (Ippen and Shank, 1975a) to produce bandwidth-limited pulses with a duration of 0.3 psec.

The shortest of all pulses are produced by the colliding-pulse-modelocked (CPM) ring laser (Fork et al., 1981). A system in our laboratory similar to that of Fork et al., is illustrated in Figure 2.8. The prism and cavity dumper have been removed to

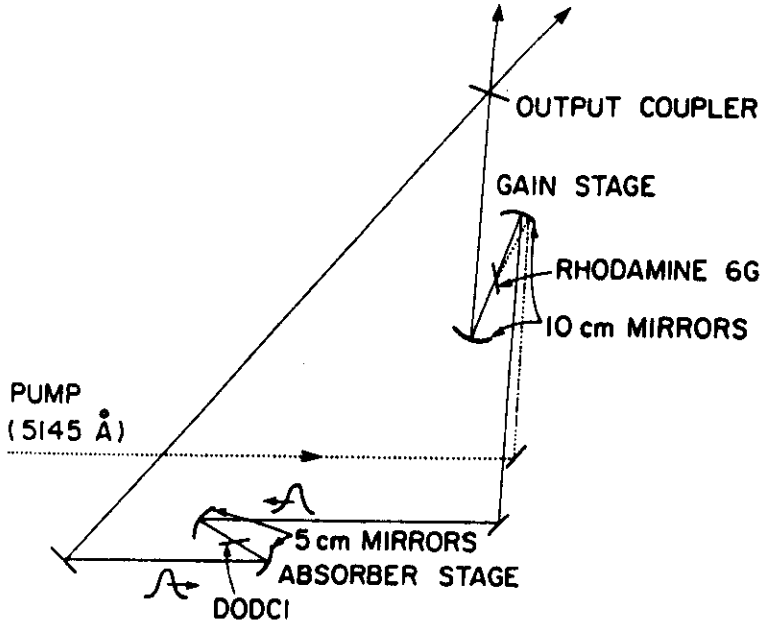

FIGURE 2.8 Femtosecond pulse generating CPM ring laser.

reduce dispersion. Since pulse collision in the saturable absorber is energetically favored (Fork et al., 1981), the RH6G gain stream is placed one-fourth of the way around the resonator so that oppositely traveling pulses are equally spaced in arrival time at the gain. The absorber stream, requiring now only DODCI, is made as thin as possible ($\sim$ 20 μm) to maximize the coherent coupling enhancement for ultrashort pulses. With a selected set of mirrors the CPM laser in our laboratory generates pulses approximately 80 fsec in duration. Similar, and even somewhat shorter, pulsewidths have been reported by Shank et al. (1982) and Halbout and Tang (1982). Output pulse duration can be greatly influenced by mirror selection which can present frustrations but may also provide opportunity for still shorter pulses.

Perhaps just as impressive as the reduction in pulsewidth achieve by CPM is the improved amplitude stability. This trans-

lates directly into improved sensitivity and signal-to-noise. Recent sampling experiments performed with this laser have demonstrated sensitivity to modulation depths of 10^{-7} (Valdmanis et al., 1982).

2.6 High Power, Sub-Picosecond Amplification

Although high repetition rate and pulse reproducibility make it possible to perform a great variety of picosecond experiments with continuously operated lasers, there are several important reasons for pushing toward higher power. Some time-resolved experiments (especially in low density systems) simply require more pulse energy. High power facilitates the conversion of pulse energy to other wavelengths for more experimental versatility. Finally, well-controlled sub-picosecond pulses make possible some very high power experiments not amenable to longer pulse durations.

An amplifier system used in our laboratory in conjunction with sub-picosecond pulses from a CPM ring laser is shown in Figure 2.9 (Migus et al., 1982; Shank et al., 1982). A frequency-doubled, Q-switched Nd:YAG is fired at optimum time for the

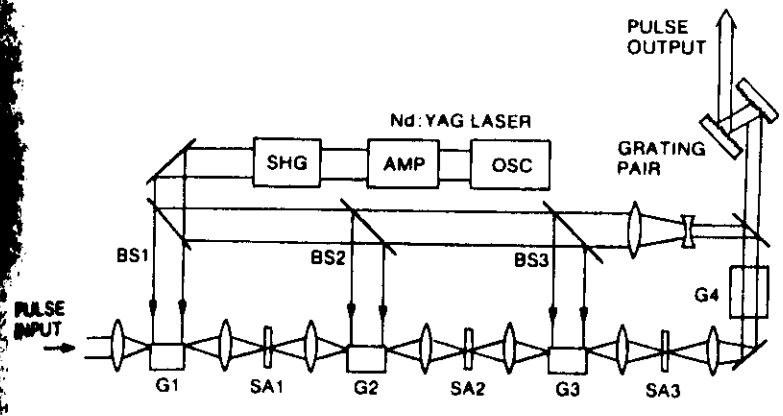

FIGURE 2.9 Four stage dye amplifier for femtosecond pulses.

selection of a single pulse from the CW dye laser. Successively larger fractions of the resulting high power pulse at 5300 Å are split off to pump four dye amplifiers. The pumping duration is about 10 nsec, synchronization with the sub-picosecond pulse is within 1 nsec, and the whole system can be operated at a rate of 10 pps.

Considerable care must be taken to prevent excessive losses due to amplified spontaneous emission (Ganiel et al., 1975). Geometrical design can be optimized to avoid self-dumping of a single stage (Wallenstein and Hansch, 1975). Strongly absorbing, malachite green, absorber streams are used to isolate stages from each other and to reshape pulses after amplification. A grating pair (see Chapter 1) is used at the output to compress the pulses by compensating for chirp introduced in the amplifiers. An optimized system such as this can produce output pulses of 80 fsec in duration and 1.2 GW peak power (Fork et al., 1982a,b).

An alternative amplification scheme for femtosecond pulses has recently been demonstrated (Kafka et al., 1982; Sizer et al., 1981). Ultrashort pulses are generated by synchronously pumping a RH6G-DQOCI (saturable absorber) dye laser with frequency-doubled pulses from a cw modelocked Nd:YAG laser. Unconverted 1.06 μm pulses from this laser are used in parallel to seed a high power Nd:YAG amplifier. The resulting intense pulses are then selected, frequency doubled, and used to pump a chain of dye amplifiers. By pumping the dye amplifiers with picosecond pulses, in synchronism with oscillator pulses to better than 50 psec, it is possible to achieve high gain with much less amplified spontaneous emission (ASE) coupling between stages. A further advantage of this picosecond synchronized system is its adaptability to higher repetition rate amplifiers (Kafka et al., 1982).

2.7 Continuum Generation

For spectroscopic purposes, high power pulses can be used to generate other wavelengths by stimulated Raman scattering, parametric conversion, or continuum generation. The latter technique (Alfano and Shapiro, 1970, 1971) is perhaps the most dramatic. By focusing amplified pulses into a cell containing H_2O, D_2O, or CCl_4 we have generated subpicosecond (continuum) pulses with a wavelength content extending from the near ultra-violet (∿ 300 nm) to the infrared (∿ 1.6 μm). Measurements on selected portions of this continuum show sub-picosecond pulse durations. With all reflective optics and generation in a thin (300 μm) jet of ethylene glycol, continuum pulses as short as 65 fsec and with negligible chirp over a broad range have been demonstrated (Fork et al., 1982b). This continuum, with an optical multichannel analyzer to obtain high resolution time spectra (Shank et al., 1978a), is now being applied to a variety of molecular and solid state studies.

Alfano, R.R., and S.L. Shapiro, 1970, Phys. Rev. Lett. 24, 584.

Alfano, R.R., and S.L. Shapiro, 1971, Chem. Phys. Lett. 3, 407.

Attwood, D.T., L.W. Coleman, M.J. Boyle, J.T. Larsen, D.W. Phillion, and K.R. Manes, 1977, Phys. Rev. Lett. 38, 282.

Aumiller, G.D., 1982, Opt. Commun. 41, 115.

Ausschnitt, C.P., and R.K. Jain, 1978, Appl. Phys. Lett. 32, 727.

Bloom, D.M., L.F. Mollenauer, C. Lin, D.W. Taylor, and A.M. DelGaudio, 1979, Opt. Lett., 297.

Bradley, D.J., New, G.H.C., and S.J. Caughey, 1970, Opt. Commun. 2, 41.

Campillo, A.J., R.C. Hyer, and S.L. Shapiro, 1979, Opt. Lett. 4, 325.

DeMaria, A.J., D.A. Stetser, and H. Heynau, 1966, Appl. Phys. Lett. 8, 22.

Duguay, M.A., J.W. Hansen, and S.L. Shapiro, 1970, IEEE J. Quant. Electron.

Eckhardt, R.C., C.H. Lee, and J.N. Bradford, 1974, Opto. Electron. 6, 67.

Eilenberger, D.J., E. Isaacs, and G.D. Aumiller, 1982, to be published.

Fendt, A., W. Kranitsky, A. Laubereau, and W. Kaiser, 1979, Opt. Commun. 24, 237.

Fork, R.L., B.I. Greene, and C.V. Shank, 1981, Appl. Phys. Lett. 38, 671.

Fork, R.L., C.V. Shank, and R.T. Yen, 1982a, Appl. Phys. Lett. 41, 273.

Fork, R.L., C.V. Shank, R.T. Yen, and C. Hirlimann, 1982b, *Picosecond Phenomena III* (Springer Verlag).

Ganiel, U., A. Hardy, G. Neumann, and D. Treves, 1975, IEEE J. Quant. Electron. QE-11, 881.

Gellerman, W., F. Luty, and C.R. Pollack, 1981, Opt. Commun. 39, 391.

Glenn, W.H., 1975, IEEE J. Quant. Electron. QE-11, 8.

Halbout, J.M., and C.L. Tang, 1982, Appl. Phys. Lett. 40, 765.

Halbout, J.M., A. Olsson, and C.L. Tang, 1981, Appl. Phys. Lett. 39, 463.

Haus, H.A., 1982b, unpublished.

Heritage, J.P., 1980, *Picosecond Phenomena II* (Springer Verlag), 343.

Heritage, J.P., and R. Jain, 1978, Appl. Phys. Lett. 32, 101.

Heritage, J.P., and E.D. Isaacs, 1981, Technical Digest CLEO.

Heritage, J.P., E. D. Isaacs, and E.P. Ippen, 1981, unpublished.

Heritage, J.P., D.S. Chemla, and P.F. Liao, 1982, *Picosecond Phenomena III* (Springer Verlag).

Ippen, E.P., and C.V. Shank, 1975a, Appl. Phys. Lett. 27, 488.

Ippen, E.P., C.V. Shank, and A. Dienes, 1972, Appl. Phys. Lett. 21, 348.

Ippen, E.P., C.V. Shank, and A. Bergman, 1976, Chem. Phys. Lett. 38, 611.

Jain, R., and J.P. Heritage, 1975, Appl. Phys. Lett. 32, 41.

Kafka, J.D., T. Sizer, C.W. Gabel, and G. Mourou, 1982, *Picosecond Phenomena III* (Springer Verlag).

Kaiser, W., and A. Laubereau, 1977, *Nonlinear Optics*, edited by Harper and Wherrett (Academic Press), 257.

Kaiser, W., A. Fendt, W. Kranitzky, and A. Laubereau, 1980, Phil. Trans. R. Soc. (London) A298, 267.

Korobkin, V.A., A.A. Malyutin, and A.M. Prokhorov, 1970, JETP Lett. 12, 150.

Kryukov, P.G., and V.S. Letokhov, 1972, IEEE J. Quant. Electron. QE-8, 766.

Kuhl, J., R. Lambrich, and D. von der Linde, 1977, Appl. Phys. Lett. 31, 657.

Laubereau, A., L. Greiter, and W. Kaiser, 1974, Appl. Phys. Lett., 25, 87.

Migus, A., C.V. Shank, E.P. Ippen, and R.L. Fork, 1982, IEEE J. Quant. Electron. QE-18, 101.

Mollenauer, L.F., and D.M. Bloom, 1979, Opt. Lett. 4, 247.

Mollenauer, L.F., N.D. Vieiro, and L. Szeto, 1982, to be published.

Saintjes, J., C.Y. She, R.C. Eckhardt, N.E. Karangelen, R. Andrews, and R. Elton, 1977, Appl. Phys. Lett. 30, 489.

Seilmeier, A., K. Spanner, A. Laubereau, and W. Kaiser, 1978, Opt. Commun. 24, 237.

Shank, C.V., and E.P. Ippen, 1975, Appl. Phys. Lett. 26, 62.

REFERENCES (continued)

Shank, C.V., R.L. Fork, R.F. Leheny, and J. Shah, 1978, Phys. Rev. Lett. 42, 112.

Shank, C.V., R.L. Fork, and R.T. Yen, 1982, *Picosecond Phenomena III* (Springer Verlag).

Shapiro, S.L., 1977, *Ultrashort Light Pulses* (Springer Verlag), chapters 2 and 3.

Shapiro, S.L., R.R. Cavanaugh, and J.C. Stephenson, 1981, Opt. Lett. 6, 471.

Siegman, A.E., 1973, IEEE J. Quant. Electron. QE-9, 247.

Sizer, T., J.D. Kafka, A. Krisiloff, and G. Mourou, 1981, Opt. Commun. 39, 259.

Vanherzeele, H. and A.E. Siegman, 1982, Technical Digest CLEO.

Von der Linde, D., 1972, IEEE J. Quant. Electron. QE-8, 328.

Von der Linde, D., O. Bernecker, and A. Laubereau, 1970, Opt. Commun. 2, 215.

Wallenstein, R. and T.W. Hansch, 1975, Opt. Commun. 14, 353.

Zinth, W., A. Laubereau and W. Kaiser, 1977, Opt. Commun. 22, 161.

THREE-PULSE-SCATTERING FOR FEMTOSECOND DEPHASING STUDIES: THEORY AND EXPERIMENT

A.M. Weiner*, S. De Silvestri** and E.P. Ippen

Department of Electrical Engineering and Computer Science
and Research Laboratory of Electronics
Massachusetts Institute of Technology
Cambridge, MA 02139

ABSTRACT

A novel transient three-pulse scattering technique for measuring ultrafast dephasing times in condensed matter is analyzed using a perturbative solution of the density matrix equation. The advantages of this technique include sub-pulsewidth resolution, a clear distinction between homogeneous and inhomogeneous broadening and sensitivity to spectral cross-relaxation. Its application to the case of a multilevel resonance is also considered. We report results of femtosecond dephasing experiments with dye molecules in liquids and in a polymer host. The dephasing time is determined to be less than 20 fsec for dyes in solution at room temperature. At low temperatures in polymers, a transition from homogeneous to inhomogeneous broadening has been observed and studied as a function of temperature.

* Permanent Address: Bell Communications Research, Holmdel, N.J. 07733

**Permanent address: Centro di Elettronica Quantistica e Strumentazione Elettronica del CNR Istituto di Fisica del Politecnico Milano Italy

I. Introduction

Optical dephasing experiments can be used to investigate fundamental static and dynamic properties of condensed matter and to elucidate the nature of photo-physical and photochemical interactions. Recent applications have included studies of guest-guest and guest-lattice interactions in mixed molecular crystals [1], tunneling mechanisms in low temperature amorphous solids [2] , dynamics of dye molecules in solution [3-4], and exciton localization in multiple quantum well structures [5]. In many cases of interest, dephasing may occur on a very rapid, sub-picosecond timescale and inhomogeneous broadening may obscure the true phase relaxation dynamics. A variety of nonlinear optical techniques, such as hole burning [6-9], fluorescence line narrowing [10], resonant Rayleigh scattering [3], and polarization spectroscopy [11], have been developed for frequency domain measurement of the homogeneous linewidth within an inhomogeneous broadened line. For time domain measurements, technique such as the photon echo [12-14] and two pulse self-diffraction [15] have also been valuable. We have recently developed a transient three-pulse scattering scheme which seems particularly advantageous for femtosecond dephasing studies [4,16-18]. Our method provides sub-pulsewidth resolution, clear distinction between homogeneous and inhomogeneous broadening and sensitivity to spectral cross-relaxation effects.

In this paper we present a comprehensive theory of our three-pulse scattering technique, considering both homogeneous and inhomogeneous broadening. The possibilities

of spectral cross-relaxation and of a multilevel system are also incorporated. Further, we report the application of three-pulse scattering to a study of dephasing of dye molecules, in solution and in a low-temperature polymer host, on a femtosecond time scale. The results in solution indicate the validity of the homogeneous broadening model and substantiate the predictions of our theory in this case. Inhomogeneous broadening effects are clearly evident in the low temperature polymer and demonstrate the ability of our technique to discriminate between the two broadening mechanisms.

II. Theory

A. General Formalism

The interaction geometry for three pulse scattering is illustrated in Fig. 1. The method relies on an optically induced grating formed by the interference of pulses #1 and #2. When the two pulses are separated temporally, a grating can still be formed provided that the dephasing time T_2 is sufficiently long. By measuring the grating amplitude as a function of the delay between pulses #1 and #2, one can measure the dephasing time. This is accomplished using pulse #3 as a delayed probe to scatter off the grating into background-free directions $\bar{k}_4 = \bar{k}_3 + (\bar{k}_1 - \bar{k}_2)$ and $\bar{k}_5 = \bar{k}_3 - (\bar{k}_1 - \bar{k}_2)$.

We have analyzed three-pulse scattering in an optically thin medium, using a third order density matrix expansion in the rotating wave and electric dipole approximations

[19-20]. For a three level system (an excited state coupled to a reservoir and a ground state), which is appropriate for materials such as dye molecules or semiconductors, this third order term may be written as follows:

$$\hat{\rho}_{ge}^{(3)}(\bar{r},t) \sim \int^{t} dt' \hat{E}(\bar{r},t') exp\left[\left(-\frac{1}{T_2} + i\Delta\omega\right)(t-t')\right] \times \int^{t'} dt'' \int^{t''} dt''' \left\{exp\left[-(t'-t'')/T_g\right] + exp\left[-(t'-t'')/T_e\right]\right\} \times \left\{\hat{E}^{*}(\bar{r},t'')\hat{E}(\bar{r},t''') exp\left[\left(-\frac{1}{T_2} + i\Delta\omega\right)(t''-t''')\right] + c.c.\right\} \quad (1)$$

where $\hat{E}$ and $\hat{\rho}_{ge}^{(3)}$ refer to positive frequency amplitudes, i.e. $E(\bar{r},t) = \hat{E}(\bar{r},t)exp(i\omega_L t) + c.c.$, $\rho_{ge}^{(3)}(\bar{r},t) = \hat{\rho}_{ge}^{(3)}(\bar{r},t)exp(i\omega_L t)$ and $\Delta\omega$ is the frequency detuning defined as the material resonance frequency ω_o minus the laser frequency ω_L. T_g is the ground state recovery time; T_e is the excited state relaxation time. We have assumed $T_g \gg T_e, T_2$. For the more general case in which vibrational relaxation, ground state recovery and dephasing occur on comparable timescale, the analysis becomes more complicated; but three pulse scattering can still be used to extract information about these processes. Although simple exponential dephasing (with time constant T_2) has been assumed here, an arbitrary transverse relaxation function $h_T(t)$ is easily incorporated and will be used interchangeably throughout [21] . For homogeneous broadening the polarization positive frequency amplitude $\hat{P}$ is simply the product of $\hat{\rho}_{ge}^{(3)}$ and the electric dipole matrix element; when inhomogeneous broadening is present, one must integrate the expression for $\hat{\rho}_{ge}^{(3)}$ over the distribution of resonant frequencies $g(\omega_o)$.

If we now write the electric field as a superposition of the three plane-wave input pulses of the same shape, we can identify the source terms for the scattering. Specifically, we write:

$$\hat{E}(\bar{r},t) = a_1 e(t+\tau)exp(-i\bar{k}_1\cdot\bar{r}) + a_2 e(t)exp(-i\bar{k}_2\cdot\bar{r}) + a_3 e(t-T)exp(-i\bar{k}_3\cdot\bar{r}) \quad (2)$$

where e(t) is the (complex) electric field envelope function and the a_i allow for different pulse intensities. The delay τ is positive when pulse #1 precedes pulse #2. With the restrictions that pulse #3 arrives at least several pulsewidths after pulses #1 and #2 and that the population does not change appreciably within the duration of pulse #3 (generally valid if pulse #3 arrives after any rapid excited state relaxation is complete), the polarization source term for scattering into direction $\bar{k}_4$ is written as follows:

$$\hat{P}^{(3)}_{\bar{k}_4}(\bar{r},t) \sim exp(-i\bar{k}_4\cdot\bar{r}) \int d\omega_o g(\omega_o) \int^t dt' e(t'-T) exp\left[(-\frac{1}{T_2} + i\Delta\omega)(t-t')\right] \times exp(-T/T_g)\hat{\gamma}(\tau,\Delta\omega) \quad (3a)$$

where

$$\hat{\gamma}(\tau,\Delta\omega) \sim \int_0^\infty dt'' \int^{t''} dt''' \{e^*(t'')e(t'''+\tau)exp\left[(-\frac{1}{T_2} + i\Delta\omega)(t''-t''')\right] + e(t''+\tau)e^*(t''')exp\left[(-\frac{1}{T_2} - i\Delta\omega)(t''-t''')\right]\} \quad (3b)$$

$\hat{\gamma}(\tau,\Delta\omega)$ represents the complex grating amplitude generated by the interference of the second pulse with the coherent polarization left behind by the first. The source for scattering into direction $\bar{k}_5$ can be obtained by substituting $-\tau$ in place of τ in eqs.(3). This

is equivalent to replacing $\hat{\gamma}$ with $\hat{\gamma}^*$. The actual population grating is written:

$$\gamma(\bar{r},\tau,\Delta\omega) = exp(-T/T_g) \times \{\hat{\gamma}(\tau,\Delta\omega)exp[-i(\bar{k}_1-\bar{k}_2)\cdot\bar{r}] + c.c.\} \quad (4)$$

where the maximum positive value of γ corresponds to the maximum ground state depletion.

The quantity actually measured is the total scattered energy U as a function of the delay τ between pulses #1 and #2 and is proportional to the time integral of the squared polarization:

$$U_{\bar{k}_4}(\tau) \sim \int dt |\hat{P}^{(3)}_{\bar{k}_4}(\bar{r},t)|^2 \quad (5)$$

and similarly for direction $\bar{k}_5$.

B. Homogeneous Broadening

In the case of homogeneous broadening, the scattered energy as a function of τ is proportional to the squared complex grating amplitude, i.e.

$$U_{\bar{k}_4} = U_{\bar{k}_5} \sim |\hat{\gamma}(\tau,\Delta\omega)|^2 \quad (6)$$

The scattering curves are always symmetric with respect to the delay τ between pulses #1 and #2 , independent of pulse #3. The scattered energy depends on the delay T of pulse #3 relative to the ground state recovery time T_g (see eq.(3a)). However, because the

dephasing is revealed through the shape of the scattering curve as a function of τ, we omit the $exp(-2T/T_g)$ factor in eq.(6) and following expressions.

For pulses much shorter than the dephasing time T_2, the scattered energy has the following simple form:

$$U_{\vec{k}_4} = U_{\vec{k}_5} \sim exp(-2|\tau|/T_2). \tag{7}$$

On the other hand, for pulses much longer than T_2, the expression for the scattered energy reduces to the squared envelope of the electric field autocorrelation, for both homogeneous and inhomogeneous broadening:

$$U_{\vec{k}_4} = U_{\vec{k}_5} \sim \left| \int dt e(t) e^*(t+\tau) \right|^2 \tag{8}$$

This property was used previously to measure the coherence properties of modelocked pulses [22]. Even when arbitrary pulse shapes are considered, the electric field autocorrelation function is still sufficient to characterize the scattering. This feature is particularly advantageous in the picosecond and femtosecond time domains, in which pulse shapes themselves cannot yet be directly measured. By rewriting the complex grating amplitude $\hat{\gamma}$ from eq. (3b) as a symmetrized convolution of the transverse relaxation function $h_T(\tau)$

with the electric field autocorrelation $G(\tau)$, we obtain the following expression:

$$\begin{aligned} \hat{\gamma}(\tau, \Delta\omega) \sim & \int d\tau' h_T(\tau'+\tau) exp\left[i\Delta\omega(\tau'+\tau)\right] G(\tau') + \\ & + \int d\tau' h_T^*(\tau'-\tau) exp\left[-i\Delta\omega(\tau'-\tau)\right] G^*(\tau') \end{aligned} \tag{9}$$

where $G(\tau') = \int dt e(t) e^*(t+\tau')$ and $h_T(\tau)$ is zero for negative values of τ. Because the electric-field autocorrelation function is readily measured [4], fast dephasing times can be resolved by looking for small differences between the scattering data and $|G(\tau)|^2$, which represents the response for $T_2 = 0$. Furthermore, because $|G(\tau)|^2$ depends not on the pulsewidth but on the pulse coherence, resolution well below the pulsewidth can be achieved using spectrally broadened pulses.

Equation (9) can be restated more elegantly in the frequency domain; the Fourier transform of the complex grating amplitude $\hat{\gamma}$ is the product of the absorption spectrum $\alpha(\omega)$ and the laser power spectrum $\phi(\omega)$:

$$\hat{\gamma}(\tau, \Delta\omega) \sim \int d\Omega exp(i\Omega\tau) \alpha(\omega_L + \Omega) \phi(\omega_L + \Omega) \tag{10}$$

where ω_L is the laser carrier frequency and $\Omega = \omega - \omega_L$. The derivation of eq. (10) is based on the Fourier transform relationships between the laser power spectrum and the electric field autocorrelation and between the absorption spectrum and the phase relaxation function, respectively.

Figure 2 shows calculated curves for the scattering produced by Gaussian pulses $e(t) = exp(-t^2/t_p^2)$ in a homogeneously broadened medium with simple exponential dephasing.

The laser frequency is exactly coincident with the material resonance. Dephasing times as short as 0.3 t_p should be observable, provided that a 10% broadening of the squared electric field autocorrelation can be measured. Assuming a pulse duration of 70 fsec full-width half-maximum (FWHM), this corresponds to a resolution of 20 fsec. In practice the resolution will depend on the experimental signal-to-noise ratio and on the accuracy of the instantaneous response measurement. Based on our previous experimental results, resolution down to 20 fsec is indeed feasible [4,16-18].

Figure 3 shows off-resonance scattering curves for Guassian pulses for a fixed $T_2 = 2.5t_p$ but for various frequency offsets $\Delta\omega t_p/2\pi$. As the detuning is increased, the scattering curve deviates from the $\Delta\omega = 0$ curve and eventually approaches the instantaneous response. For intermediate frequency offsets ($i.e. \Delta\omega t_p/2\pi \sim 0.5$) the scattering curve can actually be narrower than the $T_2 = 0$ responce. This behavior can be explained on the basis of eq. (10). For large detunings only the wings of the Lorentzian, which are very flat far from line center, are of importance. In this case the product in eq. (10) is dominated by the power spectrum, and the scattering reflects the pulse charactristics only. The narrower scattering curves calculated for intermediate detunings arise because of the positive curvature of the absorption at these frequencies. Note that the off-resonant behavior discussed above may not be of general validity but depends on the assumed Lorentzian lineshape.

C. Inhomogeneous Broadening

In the case of inhomogeneous broadening, the scattering curves are asymmetric in τ, in contrast to those for homogeneous broadening. This asymmetry provides a simple criterion for differentiating between the two types of line broadening. For an inhomogeneously broadened system, pulses #1 and #2 create a series of population gratings $\gamma(\Delta\omega)$, spatially shifted with respect to each other because of the different sub-group frequencies. This is particularly evident from eq.(4), evaluated for the case of delta-function pulses:

$$\gamma(\bar{r}, \tau, \Delta\omega) \sim exp(-|\tau|/T_2) cos\left[(\bar{k}_1 - \bar{k}_2)\cdot\bar{r} - \Delta\omega\tau\right] \tag{11}$$

If the inhomogeneous broadening is large, the total population may become almost uniform spatially. Nevertheless, scattering may still occur, as follows. The arrival of pulse #3 at time T generates for each grating a third order polarization, whose initial phase is determined by the spatial shift of the grating and which oscillates at the appropriate resonant frequency. The total polarization, again for delta function pulses, is obtained for each scattering direction from eqs.(3) using eq.(11):

$$\begin{aligned}(\hat{P}^{(3)}_{\bar{k}_4} + \hat{P}^{(3)}_{\bar{k}_5}) \sim & exp\left[-(t - T + |\tau|)/T_2\right] \int d\omega_o g(\omega_o) \\ & \left\{exp\left\{-i\left[\bar{k}_4\cdot\bar{r} - \Delta\omega(t - T + \tau)\right]\right\} + \right. \\ & \left. + exp\left\{-i\left[\bar{k}_5\cdot\bar{r} - \Delta\omega(t - T - \tau)\right]\right\}\right\}\end{aligned} \tag{12}$$

At time $T + |\tau|$, all the polarization components interfere constructively to form a phased array for radiation in direction $\bar{k}_4$ for $\tau < 0$ or in direction $\bar{k}_5$ for $\tau > 0$. Thus, for a

fixed value of τ, scattering occurs preferentially in a single direction. In the limit of T_2 much longer than the inverse inhomogeneous width (wide inhomogeneous broadening), we obtain the following expression for the scattered energy:

$$\tau \geq 0 : U_{\bar{k}_4} = 0; U_{\bar{k}_5} \sim exp(-4\tau/T_2) \tag{13a}$$

$$\tau \leq 0 : U_{\bar{k}_4} \sim exp(4\tau/T_2); U_{\bar{k}_5} = 0 \tag{13b}$$

Note that the inhomogeneous limit of our three pulse scattering technique gives the same result as the weak-field limit of the stimulated photon echo [13]. We wish though to emphasize the generality of three pulse scattering, which includes both the homogeneous and inhomogeneous limits within its framework.

Figure 4 shows calculated curves for the scattering of Gaussian pulses into direction $\bar{k}_5$, in the case of wide inhomogeneous broadening. The characteristic exponential decay is evident only for $T_2 > 2t_p$. Even for small dephasing times, however, the rising edge and peak of these scattering curves exhibit a pronounced shift towards positive delay with increasing T_2. The normalized peak shift τ_s (defined as the total separation between the peaks of the $\bar{k}_4$ and $\bar{k}_5$ scattering curves normalized to t_p) is plotted in Fig. 5 as a function of T_2/t_p. The graph is close to linear for $T_2 < t_p$ with $\tau_s \sim T_2$. Thus, τ_s can serve as a sensitive measure of dephasing times shorter than the pulsewidth.

As in the case of homogeneous broadening, the electric field autocorrelation alone

is sufficient to provide a reference for the three-pulse scattering. In the limit of wide inhomogeneous broadening, substitution of eq. (9) into eq. (3) yields after some further simplification the following:

$$\tilde{P}^{(3)}_{\bar{k}_4}(\bar{r},t) \sim exp(-i\bar{k}_4 \cdot \bar{r}) \int dt' |h_T(t-t')|^2 q(t'-T) G^*(t-t'+\tau) \tag{14}$$

We have written $q(t'-T)$ instead of $e(t'-T)$ as previously to allow for the possibility that the shape of pulse #3 differs from that of the other two pulses. The scattered energy is evaluated using eq. (14) in eq. (5), with the following result:

$$U_{\bar{k}_4}(\tau) \sim \int\int d\tau' d\tau'' |h_T(\tau')|^2 |h_T(\tau'')|^2 Q(\tau'-\tau'') G^*(\tau+\tau') G(\tau+\tau'') \tag{15}$$

where $Q(\tau) = \int dt q(t) q^*(t+\tau)$. Equation (15) demonstrates that the scattering curves depend directly on the experimentally accessible electric field autocorrelation functions, as claimed. Also in the case of an arbitrary inhomogeneous distribution, the scattered energy can be expressed entirely in terms of the field autocorrelation; however, the formula is rather cumbersome and is not given here.

D. Spectral Cross – relaxation

We consider now the possibility of spectral cross-relaxation within an inhomogeneously broadened line, which arises when the resonant frequencies of individual absorbers are not fixed but can migrate within the inhomogeneous distribution. In the presence of spectral

cross-relaxation, the scattering behavior is sensitive to the delay T of pulse #3. For delays longer than the characteristic spectral diffusion time ($T >> T_3$), the rephasing discussed in connection with eq. (12) can no longer occur since the various gratings are no longer distinct. There exists then only a total population grating, whose amplitude is equal to the sum of the individual complex grating amplitudes, expressed according to eq. (9) and weighted by the inhomogeneous distribution, as follows:

$$\hat{\gamma}_{TOTAL}(\tau) \sim \int d\omega_o g(\omega_o)\hat{\gamma}(\tau, \Delta\omega) \tag{16}$$

This expression simplifies considerably upon substitution of eq. (10) for the individual complex grating amplitudes, with the result:

$$\hat{\gamma}_{TOTAL}(\tau) \sim \int d\Omega exp(i\Omega\tau)\alpha_{TOTAL}(\omega_L + \Omega)\phi(\omega_L + \Omega) \tag{17}$$

Here $\alpha_{TOTAL}(\omega) = \int d\omega_o g(\omega_o)\alpha_{HOM}(\omega - \omega_o)$ is the total absorption lineshape, given by the convolution of inhomogeneous distribution with the baseband homogeneous lineshape function α_{HOM}. Equation (17) is exactly analogous to eq. (10) for homogeneous broadening. Thus, for $T \gg T_3$, the scattered energy is a symmetric function of τ; however, the width of the scattering curve reflects the inverse absorption width rather than the actual dephasing time T_2.

We have investigated analytically the transition from asymmetric to symmetric scattering curves with increasing T/T_3 for the case of delta-function pulses and a Gaussian

inhomogeneous distribution $g(\omega_o) = (1/\delta\omega\sqrt{\pi})exp\left[-(\omega - \omega_o)^2/\delta\omega^2\right]$. The probability per unit time that an absorber initially resonant at ω_o' jumps to a new resonant frequency ω_o is assumed to have the following simple form [23]:

$$p(\omega_o' \rightarrow \omega_o) = g(\omega_o)/T_3. \tag{18}$$

Scattering curves for direction $\bar{k}_5$ are shown in Fig. 6 as a function of τ for several values of the pulse #3 delay T/T_3, assuming $\delta\omega T_2 = 10$ and that the ground state recovery time T_g is much longer than the time scale of interest. As the delay of the third pulse is increased, the scattering curves become narrower but more symmetric. The scattering efficiency for $\tau = 0$ is insensitive to the spectral diffusion since all gratings are created in phase.

According to the discussion above, three pulse scattering can yield information about spectral diffusion as well as dephasing. This is accomplished by repeating the experiment for various settings of T and looking for a transition from asymmetric to symmetric scattering curves. The ability to investigate spectral diffusion using our transient three pulse technique constitutes an advantage over recently proposed techniques which use incoherent light [24-25].

E. Multilevel Systems

We have already seen how the three-pulse scattering can be sensitive to spectral cross-relaxation. We discuss now a further potential complication which arises when a multilevel

rather than a two-level energy structure is appropriate. When several transitions are excited simultaneously, interference between the various coherences leads to dephasing faster than that due to one line individually. Unlike inhomogeneous broadening dephasing due to multi-line excitation is an irreversible process.

We have considered analytically a simplified multilevel model in which the ground state is still an isolated level but in which the excited state consists of a set of discrete lines, each with its own matrix element and dephasing rate. Each individual transition is assumed homogeneously broadened. The possibility of a smooth, unresolved absorption spectrum or of a continuum is included as a special case (when the individual homogeneous linewidths exceed the level spacing). Even for a general homogeneously broadened multilevel system, we find that the scattering is still a symmetric function of τ (with the same restrictions as previously on the delay of pulse #3). The scattering curves may be calculated by eq. (10) in a fashion exactly analogous to the homogeneously broadened two-level system, except that now the total absorption spectrum, rather than that due to a single line, must be used. Thus, when the individual transitions are unresolved even in the absence of any inhomogeneous broadening, three pulse scattering yields an effective dephasing time which is the inverse of the total absorption width and which must not be considered an average dephasing time for the individual resonances.

This discussion does not preclude the possibility of observing inhomogeneous broad-

ening behavior in multilevel systems. For example, inhomogeneous broadening may lead to a total absorption spectrum still wider than the multi-level absorption spectrum of an individual absorber. Alternately, inhomogeneous broadening may result in a smooth absorption spectrum even when the spectrum of a single molecule consists of discrete, resolved lines. When inhomogeneous broadening significantly influences the multilevel absorption spectrum, asymmetric scattering curves and peak shifts may be observed.

It is interesting to compare dephasing measurements performed in the time domain (three pulse scattering) and in the frequency domain (spectral hole burning). For a two level system these techniques yield the same dephasing time. In the case of a multilevel system or of a continuum, however, temporal and spectral measurements are no longer directly related. In a homogeneously broadened, unresolved multilevel system, three pulse scattering measures a dephasing time which is the inverse of the total absorption bandwidth. A spectral hole burning experiment, however, can yield hole widths related to the linewidth of a single transition. This difference between the temporal and spectral measurement techniques must be considered when describing complex multilevel systems in terms of two-level atom concepts.

III. Experiment

As an initial application of three pulse scattering, we used pulses form a colliding-

pulse-modelocked (CPM) ring dye laser [26] to investigate the dephasing of dye molecules in solution [4,16]. Our laser produced pulses with a duration 70 fsec FWHM at a wavelength of 620 nm and with a repetition rate of 125 MHz. In the case of parallel polarization for all three pulses, the scattering amplitude was strongly enhanced due to the formation of a cumulative thermal grating. When thermal gratings dominate, our technique measures the total absorption width, independent of the actual dephasing time T_2; and scattering curves are always symmetric. Nevertheless, the thermal grating effect can be exploited to test the theory developed for the case of homogeneous broadening. Figure 7 shows parallel polarization scattering data for the dyes Nile blue and rhodamine 640 in methanol. Also shown are curves calculated on the basis of eq. (10), using the measured laser power spectrum and dye absorption spectra. In the case of Nile blue, the calculated curve is indistinguishable from the squared electric field autocorrelation, due to the shallow curvature of the absorption spectrum at the laser wavelength (which coincides with the absorption peak). In the case of rhodamine 640, the excitation is shifted 50 nm to the red of the absorption peak; in this region the absorption varies sufficiently rapidly that significant departure from the instantaneous scattering response is predicted. The excellent agreement of the calculated curves with the data in Fig. 7 demonstrates the validity of our theory in the case of homogeneous broadening, for instantaneous and noninstaneous dephasing and for resonant and off-resonant excitation. The rhodamine 640 data substantiates our claim

(see Fig.3) that scattering curves narrower than the instantaneous response may occur.

True dephasing information can be obtained if the thermal grating is eliminated using orthogonal polarizations for pulses #1 and #2. Scattering curves for Nile blue are still symmetric and indistinguishable from the instantaneous response. This indicates homogeneous broadening with an apparent dephasing time less than the 20 fsec experimental resolution. Similar results were obtained with several other dyes. This very rapid dephasing results from the simultaneous excitation of many different states within the absorption band and does not correspond to the dephasing time of an individual transition. Our experiments do show, however, that the temporal response of these molecules in solution may be modeled as homogeneously broadened at room temperature.

We have also studied the dephasing of dye molecules in thin films of PMMA polymer [18] using amplified CPM laser pulses [27] with a duration of 75 fsec FWHM and a 10 Hz repetition rate. As a preliminary experiment, we measured the grating lifetime by scanning the delay T of pulse #3 with the delay τ between pulses #1 and #2 set to zero [28]. Data are shown in Fig. 8 for two typical dyes, cresyl violet and oxazine 720, at a temperature of 15 K. The scattering is zero when pulse #3 arrives before pulse #1 and #2; this demonstrates that no persistent grating develops. For large T the scattering approaches an almost constant level (for our 2 psec delay range) that decays on a nanosecond time scale. The large peaks near $T = 0$ are an artifact which occurs when all three beams

interact coherently. The tails of the $T = 0$ peaks are evidence of intraband excited state relaxation of the dye molecules occurring on a time scale of several hundred femtoseconds. Similar rapid excited state relaxation has also been observed for several dyes molecules in liquid solution at room temperature [29].

We now proceed to a discussion of the dephasing measurements. Scattering curves for cresyl violet taken at a temperature of 15 K are shown in Fig. 9a for both scattering directions. The delay of the third pulse was set to 1.3 psec. The asymmetry of the curves, illustrated by the 60 fsec peak shift, shows that inhomogeneous broadening is present and demonstrates the ability of our technique to distinguish between homogeneous and inhomogeneous broadening. With increasing temperature the asymmetry and peak shift decrease. At room temperature the peak shift is no longer evident, as shown in the data of Fig. 9b. At this temperature homogeneous broadening apparently dominates.

To check for spectral cross-relaxation, we repeated the dephasing measurements with the delay of the third pulse varying between 200 fsec and 200 psec. The observed peak shifts of 60 fsec at 15 K and 33 fsec at 100 K were found to be independent of the third pulse delay. Thus, spectral diffusion is not evident in this time scale and temperature range.

Despite the clearly resolved peak shifts in our low temperature scattering data, we do not observe a pronounced tail indicative of a long T_2. According to the simple analysis of

Section II.C this would indicate dephasing on a time scale comparable to the pulsewidth. However, low temperature nonphotochemical hole burning measurements on cresyl violet in polyvinyl alcohol polymer indicate that the dephasing time should be on the order of one or two picoseconds [9]. Our results can be explained on the basis of a multilevel rather than a two-level energy structure. From the hole burning spectra, we infer that for our laser bandwidth several lines are indeed excited. Because the lines of a single cresyl violet molecule are well-resolved at low temperature, inhomogeneous broadening still contributes to the dephasing; and a peak shift is detected. As the temperature is increased, the individual lines broaden and eventually overlap; the molecule behaves like a homogeneously broadened two-level system with a linewidth equal to the total absorption width. This explanation applies to the room temperature data shown in Fig. 9b as well as to the room temperature data for dye molecules in solution.

In additon to cresyl violet we have also investigated the dephasing of Nile blue and oxazine 720. For both dyes the scattering curves are symmetric over our entire temperature range (15 K to 300 K), and no peak shifts are detected . The 15 K Nile blue data are shown in Fig. 10. The results are again explained in terms of a multilevel structure. For Nile blue and for oxazine 720, the laser photons have in each case an excess energy of several hundred cm^{-1} relative to the absorption onset; for cresyl violet , however, the laser frequency is coincident with the absorption edge. Therefore Nile blue and oxazine

720 should have considerably higher densities of states than does cresyl violet. Due to higher densities of states, the individual lines may not be resolved, even at 15 K. In this case, the dephasing should appear instantaneous.

IV. Summary

Using a third-order density matrix expansion, we have analysed three-pulse scattering as a method for studying ultrafast optical dephasing. The technique provides a clear distinction between inhomogeneous and homogeneous broadening , and it does so in a way that facilitates measurement of dephasing times comparable to or shorter than the pulsewidth. We have also developed the theory to include the effects of spectral cross-relaxation and the behavior of a multilevel system. By varying two of the relative delays in the three pulse geometry, we show that it is possible to monitor spectral cross-relaxation effects and to separate them from dephasing and energy relaxation phenomena. With a multilevel system three-pulse scattering exhibits the same advantages predicted for a two-level system. Unlike dephasing in an inhomogenous ensemble, however, dephasing due to excitation of multiple levels of the same molecule is irreversible; and its scattering signature is determined only by the input pulse and its multilevel absorption spectrum.

To illustrate the principal characteristics of three-pulse scattering, we have presented results of femtosecond dephasing experiments with dye molecules in liquids and in a poly-

mer host. At room temperature the results indicate apparent dephasing times of less than 20 fsec and support the contention that the dye absorption bands are homogenously broadened. At temperatures below 100 K, using cresyl violet in PMMA, we have observed asymmetric scattering due to inhomogeneous broadening. These results demonstrate the predicted sensitivity of three-pulse scattering to the two different broadening mechanisms and establish three-pulse scattering as an important tool for studies of ultrafast dephasing in condensed matter.

Acknowledgement

This research was supported in part by a grant from the Joint Services Electronics Program under contract DAAG 29-83-K-003. A.M. Weiner was a Fannie and John Hertz Foundation Graduate Fellow. S. De Silvestri is a NATO Science Fellow. We would like to acknowledge Dr. J.G. Fujimoto for valuable discussions.

References

[1] D.E. Cooper, R.W. Olson, and M.D. Fayer, "Intermolecular interaction dynamics and optical dephasing: picosecond photon echo measurements in mixed molecular crystals," J. Chem. Phys. **72**, 2332-2339 (1980).

[2] B. Golding and J.E. Graebner, "Relaxation times of tunneling systems in glasses," in Amorphous Solids, W.A. Philips, ed. (Springer-Verlag, Berlin, 1981), pp. 107-134.

[3] H. Souma, T. Yajima and Y. Taira, "Ultrafast relaxation study by resonant Rayleigh-type mixing spectroscopy using picosecond pulses," J. Phys. Soc. Jpn **48**, 2040-2047 (1980).

[4] A.M. Weiner and E.P. Ippen, "Novel transient scattering technique for femtosecond dephasing measurements," Opt. Lett. **9**, 53-55 (1984).

[5] J. Hegarty, L. Goldner, and M.D. Sturge, unpublished.

[6] J. Friedrich. H. Wolfrum, and D. Haarer, "Photochemical holes: a spectral probe of the amorphous state in the optical domain," J. Chem. Phys. **77**, 2309-2316 (1982).

[7] H.P.H. Thijssen, R. Von Den Berg and S. Volker, "Thermal broadening of optical homogeneous linewidths in organic glasses and polymers studied via photochemical hole-burning," Chem. Phys. Lett. **97**, 295-302 (1983).

[8] B.L. Fearey, T.P. Carter, and G.J. Small, "Efficient nonphotochemical hole burning of dye molecules in polymers," J. Phys. Chem. **87**, 3590-3592 (1983).

[9] T.P. Carter, B.L. Fearey, J.M. Hayes, and G.J. Small, "Optical dephasing of cresyl violet in a polyvinyl alcohol polymer by non-photochemical hole burning," Chem. Phys. Lett. **102**, 272-276 (1983).

[10] A. Szabo, "Observation of the optical analog of the Mossbauer effect in ruby," Phys. Rev. Lett. **27**, 323-326 (1971).

[11] M.D. Levenson, R.M. MacFarlane, and R.M. Shelby, "Polarization-spectroscopy measurement of the homogeneous linewidth of an inhomogeneously broadened color-center band," Phys. Rev. **B22**, 4915-4929 (1980).

[12] I.D. Abella, N.A. Kurnit, and S.R. Hartmann, "Photon echoes," Phys. Rev. **A141**, 391-406 (1966).

[13] T. Mossberg, A. Flusberg, R. Kachru, and S.R. Hartmann, "Total scattering cross section for Na on He measured by stimulated photon echoes," Phys. Rev. Lett. **42**, 1665-1669 (1979).

[14] W.H. Hesselink and D.A. Wiersma, "Picosecond photon echoes stimulated from an accumulated grating," Phys. Rev. Lett. **43**, 1991-1994 (1979).

[15] T. Yajima, Y. Ishida and Y. Taira, "Investigation of subpicosecond dephasing processes by transient spatial parametric effect in resonant media," in Picosecond Phenomena II R.M. Hochstrasser, W. Kaiser and, C.V. Shank, eds. (Springer-Verlag, Berlin, 1980) p.190-194

[16] A.M. Weiner, S. De Silvestri, and E.P. Ippen, "Femtosecond dephasing measurements using transient induced gratings," in Ultrafast Phenomena IV, D.H. Auston and K.B. Eisenthal, eds. (Springer-Verlag, Berlin, 1984), p. 230-232.

[17] A.M. Weiner, "Femtosecond Optical Pulse Generation and Dephasing Measurements in Condensed Matter", Sc.D. dissertation, Massachusetts Institute of Technology, 1984.

[18] S. De Silvestri, A.M. Weiner, J.G. Fujimoto and E.P. Ippen, "Femtosecond dephasing studies of dye molecules in a polymer host," Chem. Phys. Lett., in press.

[19] N. Bloembergen, Nonlinear Optics (Benjamin, Reading, Massachusetts, 1965).

[20] Y.R. Shen, The Principles of Nonlinear Optics (John Wiley & Sons, New York, 1983).

[21] R. Kubo, "A stochastic theory of line-shape and relaxation," in Fluctuations, Relaxation and Resonance in Magnetic Systems. D. ter Haar, ed. (Plenum Press, New York, 1962), p. 23-68.

[22] H.J. Eicher, U. Klein, and D. Langhans, "Coherence time measurement of picosecond pulses by a light-induced grating method," Appl. Phys. **21**, 215-219 (1980).

[23] G. Mourou, "Spectral hole burning in dye solution," IEEE J. Qantum Electron. **QE – 11**, 1-8 (1975).

[24] S. Asaka, H. Nakatsuka, M. Fujiwara, and H. Matsuoka, "Accumulated photon echoes with incoherent light in Nd^{3+}-doped silicate glass," Phys. Rev. **A29**, 2286-2289 (1984).

[25] N. Morita, T. Yajima and Y. Ishida, "Coherent transient spectroscopy with ultra-high time-resolution using incoherent light," in Ultrafast Phenomena IV, D.H. Auston and K.B. Eisenthal, eds. (Springer-Verlag, Berlin, 1984) p. 239-241.

[26] R.L. Fork, B.I. Green, and C.V. Shank, "Generation of optical pulses shorter than 0.1 psec by colliding pulse mode-locking," Appl. Phys. Lett. **38**, 671-672 (1981).

[27] R.L. Fork, C.V. Shank, and R.T. Yen, "Amplification of 70-fs optical pulses to gigawatt powers," Appl. Phys. Lett. **41**, 223-225 (1982).

[28] D.W. Phillon, D.J. Kuizenga, and A.E. Siegman, "Subnanosecond relaxation time measurements using a transient induced grating method," Appl. Phys. Lett. **27**, 85-89 (1975).

[29] A.M. Weiner and E.P. Ippen, unpublished.

Figure Captions

Fig. 1 Interaction scheme for dephasing measurements by the three-pulse scattering technique.

Fig. 2 Calculated scattered energy for Gaussian pulses as a function of the normalized delay τ/t_p between pulse #1 and #2, in a homogeneously broadened medium for several values of T_2/t_p. The laser frequency is on resonance.

Fig. 3 Off-resonance scattering curves for Gaussian pulses as a function of τ/t_p for various frequency offsets $\Delta\omega t_p/2\pi$. The dephasing time T_2 was set to 2.5 t_p.

Fig. 4 Calculated scattered energy, for Gaussian pulses as a function of τ/t_p for different values of T_2/t_p in the case of wide inhomogeneous broadening.

Fig. 5 Normalized peak shift τ_s/t_p as a function of the normalised dephasing time T_2/t_p.

Fig. 6 Calculated scattered energy for delta-function pulses as a function of τ/T_2 for different values of T/T_3, in a inhomogeneously broadened medium with $\delta\omega T_2 = 10$. $T_g \gg T$ is assumed.

Fig. 7 Scattering data for rhodamine 640 and Nile blue in methanol, using parallel polarization.

Fig. 8 Scattered energy for (a) cresyl violet and (b) oxazine 720 in PMMA at 15 K as a function of the delay T of pulse #3. Pulses #1 and #2 are set at zero relative delay.

Fig. 9 Scattered energy for cresyl violet in PMMA as a function of delay τ between pulses

#1 and #2. The temperatures are: a) 15 K, b) 290 K. The delay of pulse #3 was set to 1.3 psec.

Fig. 10 Scattered energy for Nile blue in PMMA at 15 K as a function of the delay τ between pulses #1 and # 2. The delay of pulse #3 was set to 1.3 psec.

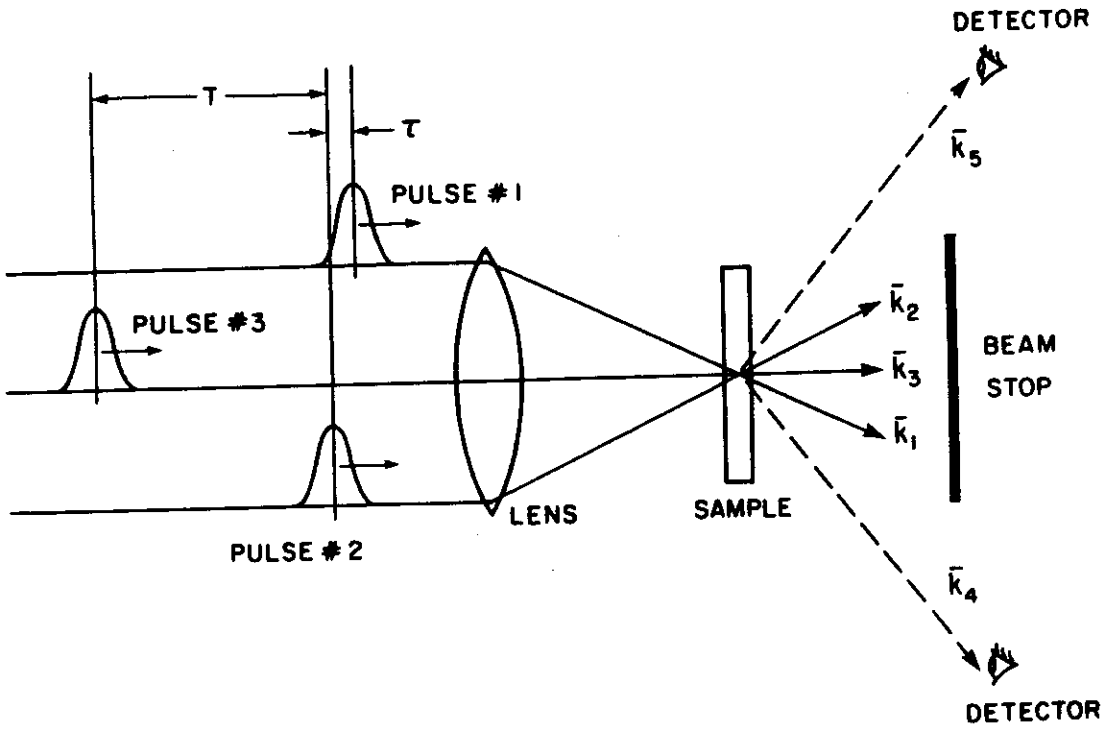
DETECTOR
T
τ
PULSE #1
PULSE #3
PULSE #2
LENS
SAMPLE
$\bar{k}_5$
$\bar{k}_2$
$\bar{k}_3$
$\bar{k}_1$
BEAM
STOP
$\bar{k}_4$
DETECTOR

Fig 1

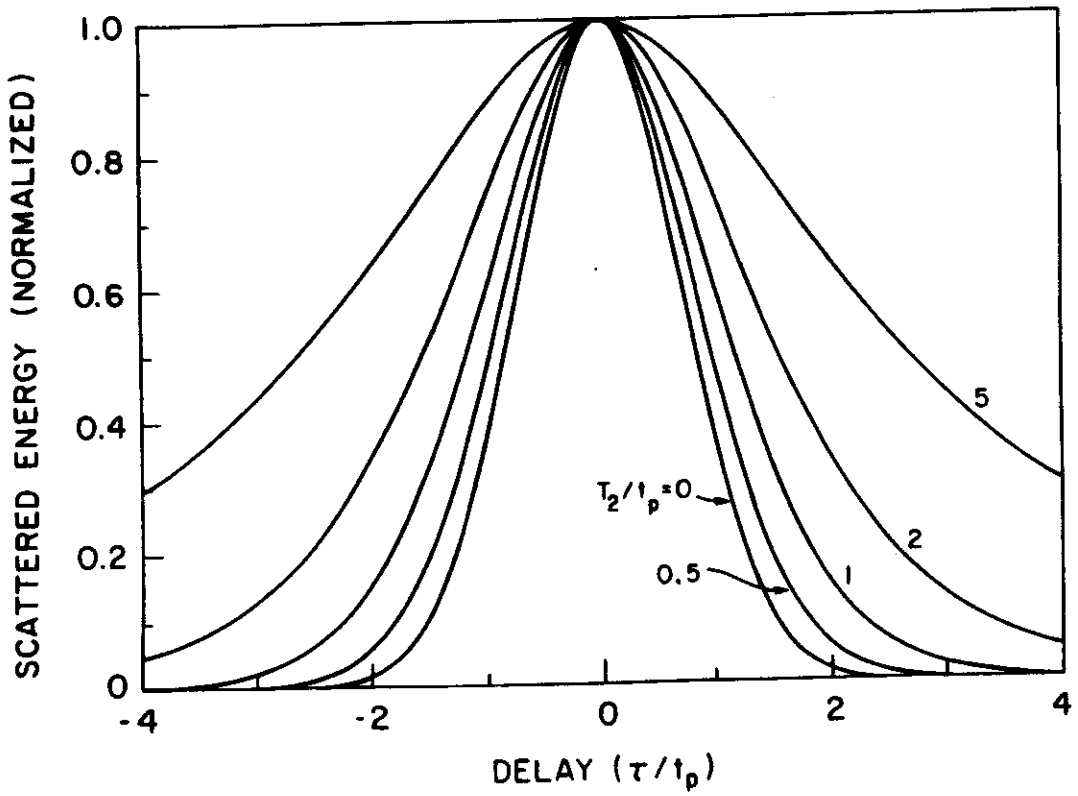
SCATTERED ENERGY (NORMALIZED)
1.0
0.8
0.6
0.4
0.2
0
-4
-2
0
2
4
DELAY (τ/t_p)
T_2/t_p=0
0.5
1
2
5

Fig.2

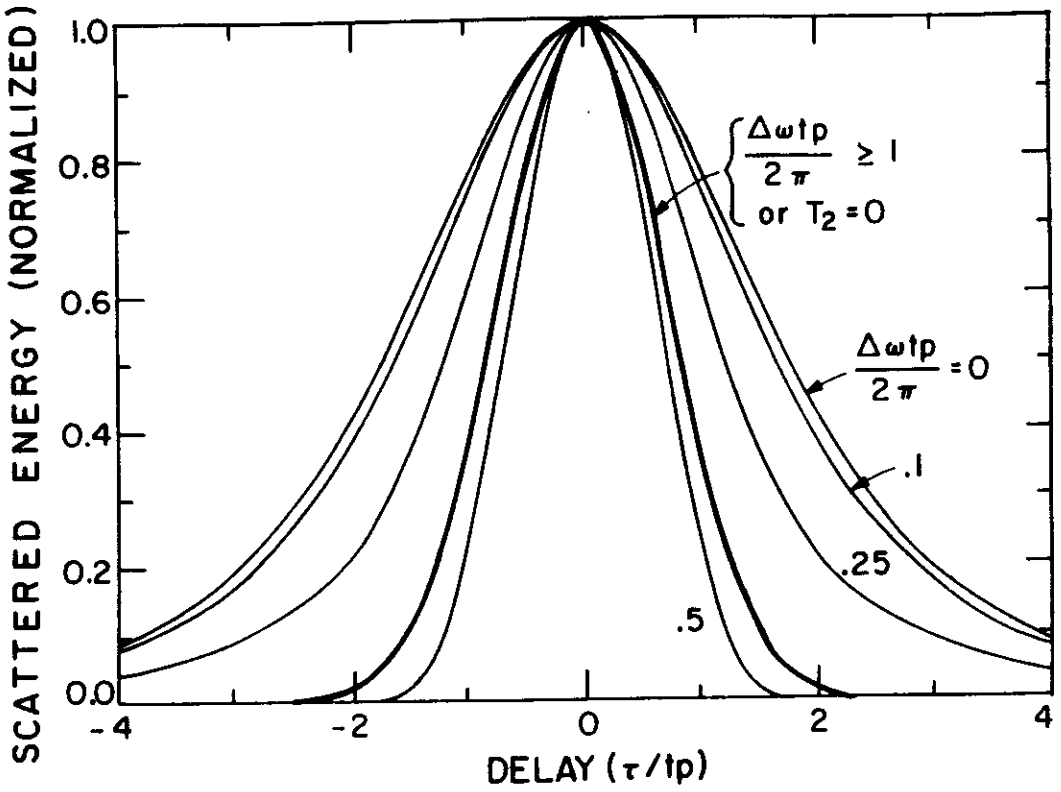
SCATTERED ENERGY (NORMALIZED)
1.0
0.8
0.6
0.4
0.2
0.0
-4
-2
0
2
4
DELAY (τ/tp)
Δωtp/2π ≥ 1
or T2 = 0
Δωtp/2π = 0
.1
.25
.5

Fig 3

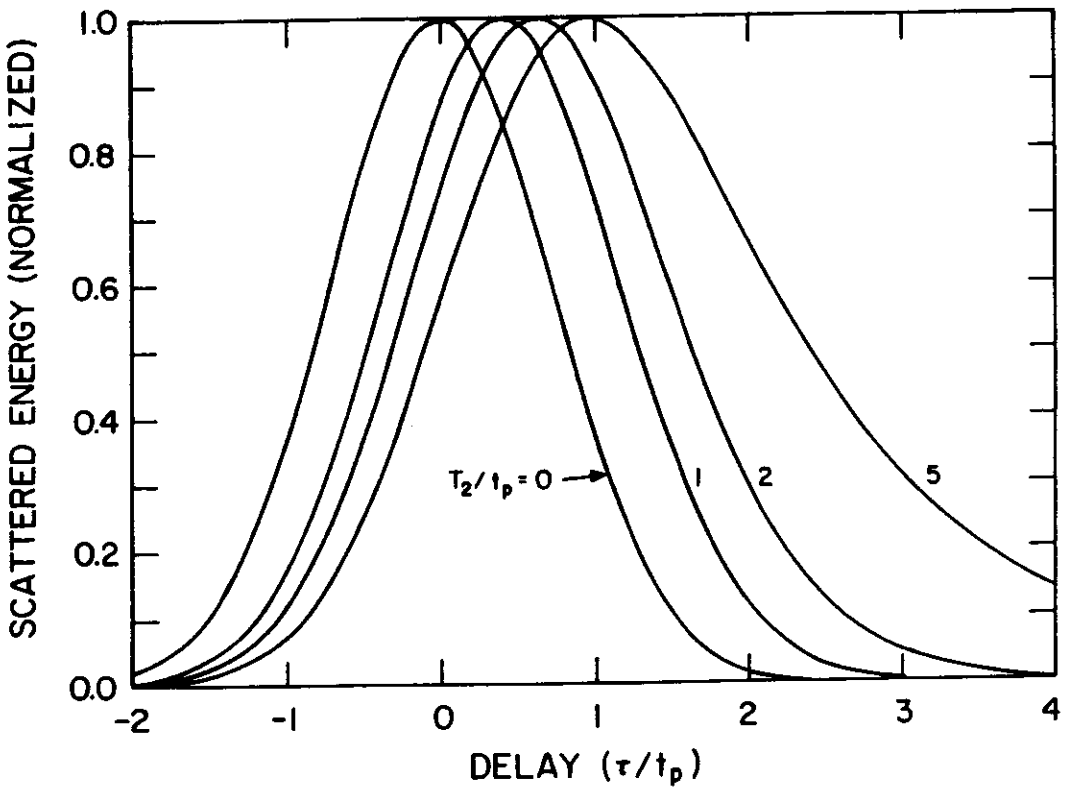
SCATTERED ENERGY (NORMALIZED)
1.0
0.8
0.6
0.4
0.2
0.0
-2
-1
0
1
2
3
4
DELAY (τ/tp)
T2/tp = 0
1
2
5

Fig.4

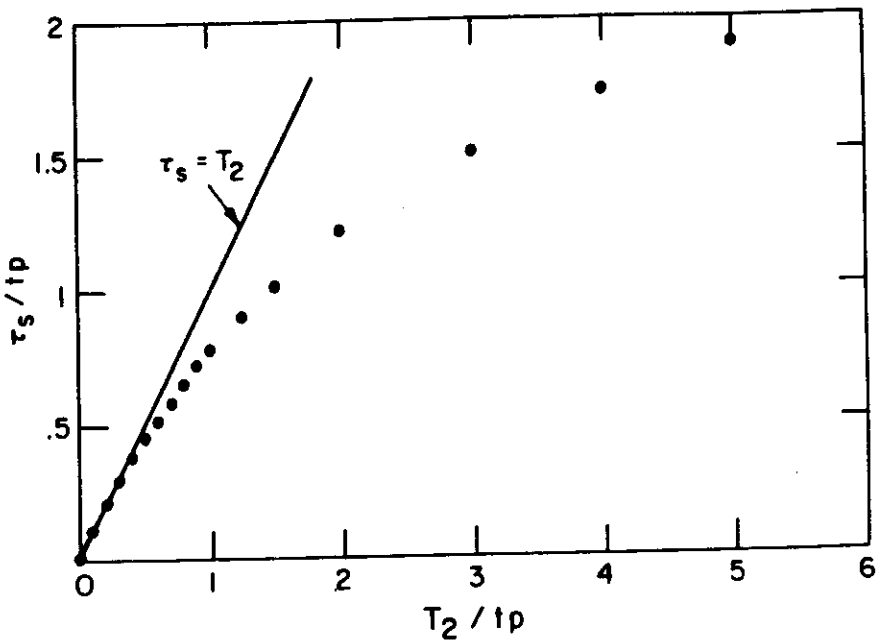
2
1.5
1
.5
$\tau_s = T_2$
τ_s / tp
0
1
2
3
4
5
6
T_2 / tp

Fig.5

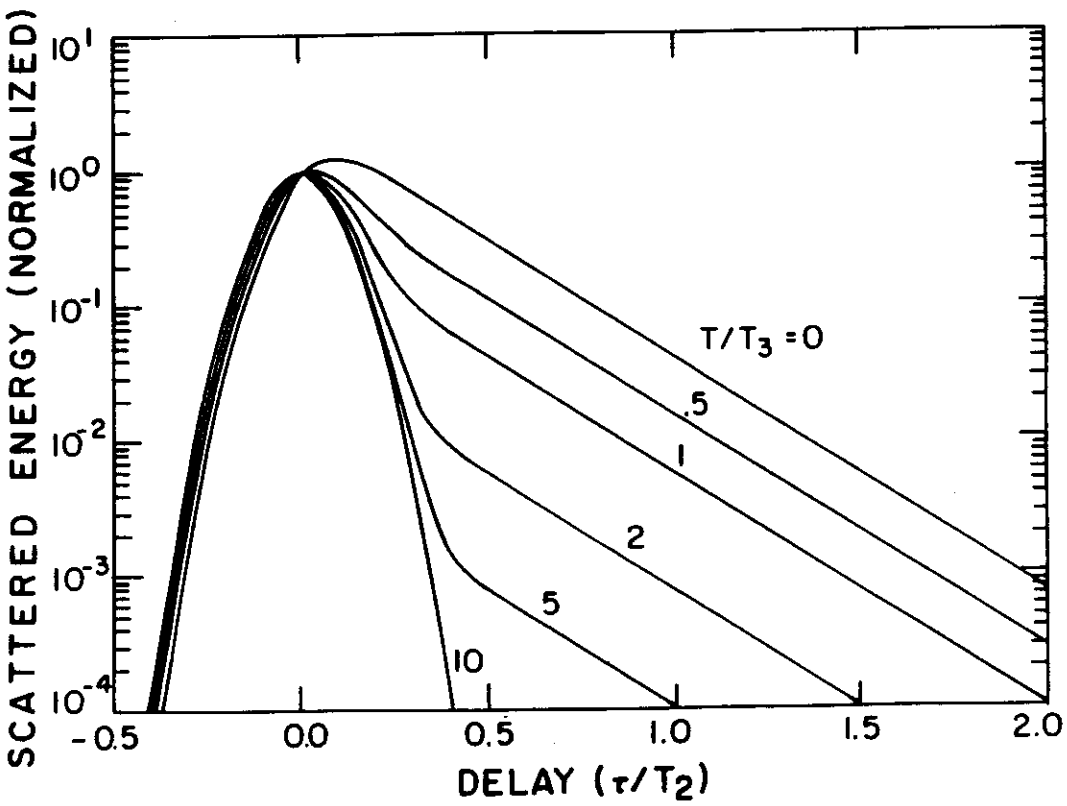
SCATTERED ENERGY (NORMALIZED)
10^{1}
10^{0}
10^{-1}
10^{-2}
10^{-3}
10^{-4}
$T/T_3 = 0$
.5
1
2
5
10
-0.5
0.0
0.5
1.0
1.5
2.0
DELAY (τ/T_2)

Fig.6

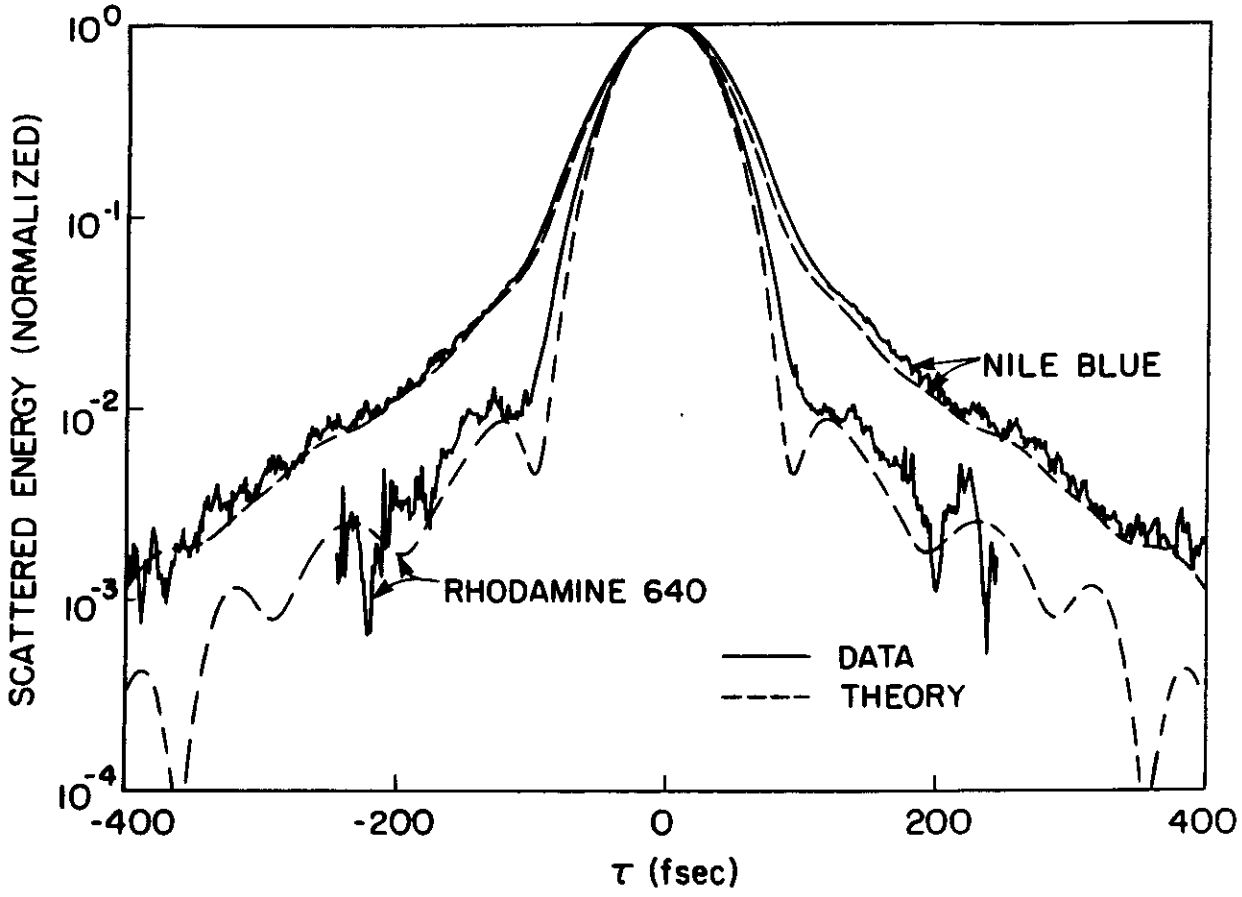
SCATTERED ENERGY (NORMALIZED)
10^0
10^{-1}
10^{-2}
10^{-3}
10^{-4}
-400
-200
0
200
400
τ (fsec)
NILE BLUE
RHODAMINE 640
DATA
THEORY

Fig.7

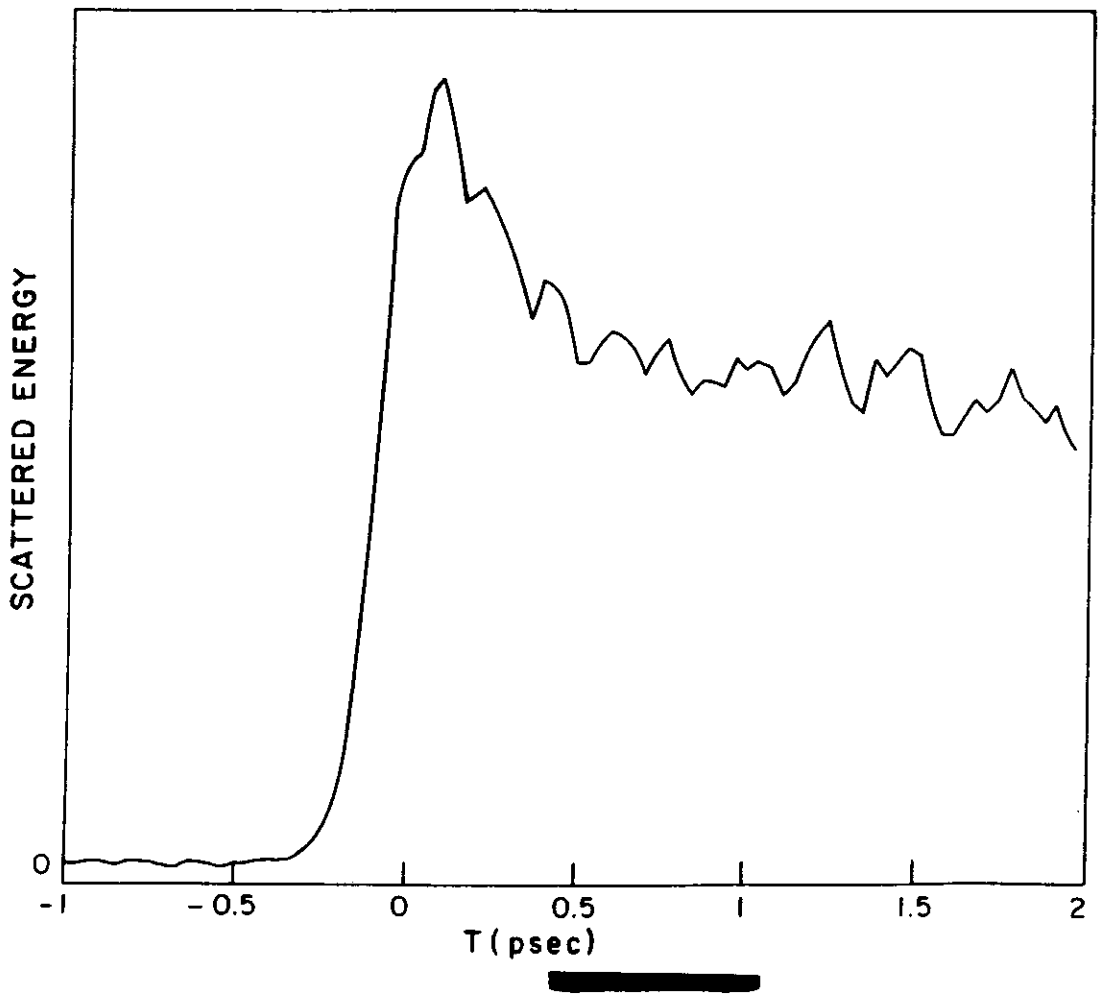
SCATTERED ENERGY
0
-1
-0.5
0
0.5
1
1.5
2
T (psec)

Fig 8a

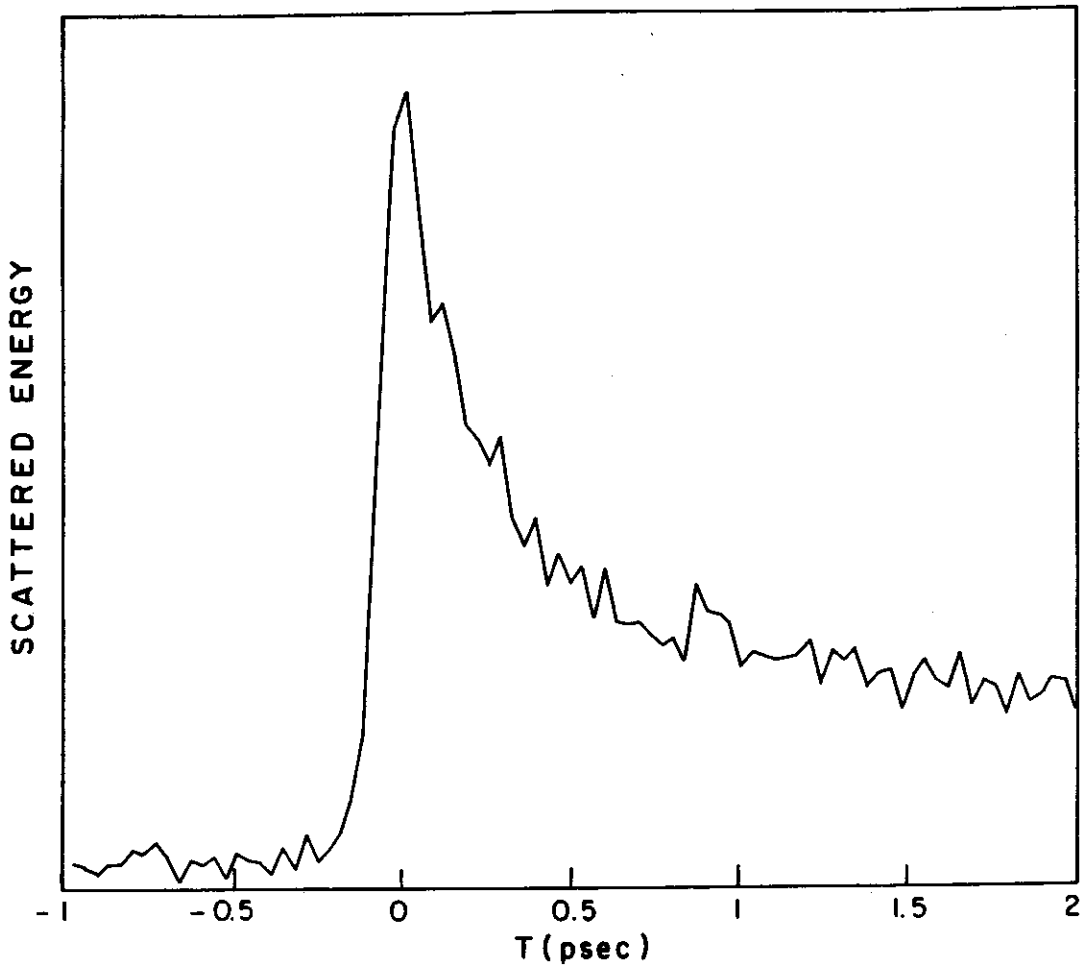
SCATTERED ENERGY
-1
-0.5
0
0.5
1
1.5
2
T (psec)

Fig 8b

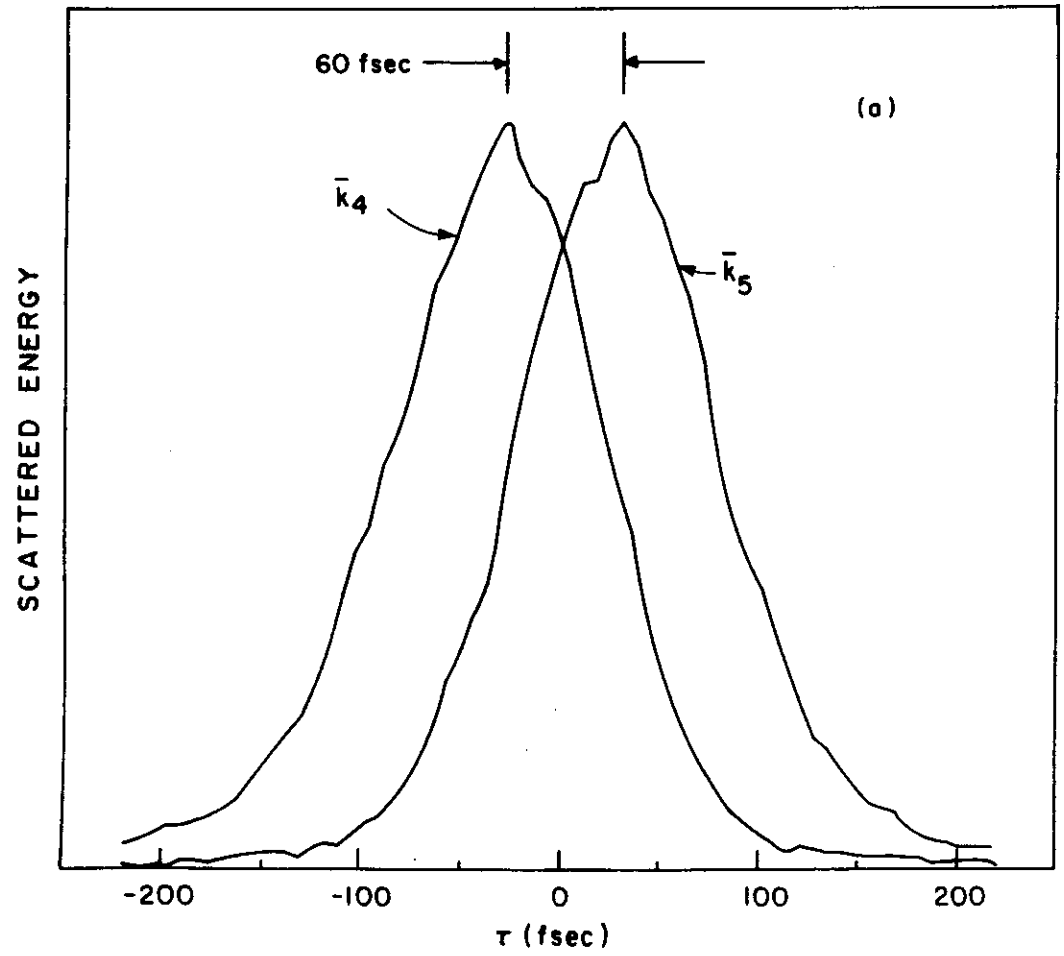
60 fsec
(a)
$\bar{k}_4$
$\bar{k}_5$
SCATTERED ENERGY
-200
-100
0
100
200
τ (fsec)

Fig 9a

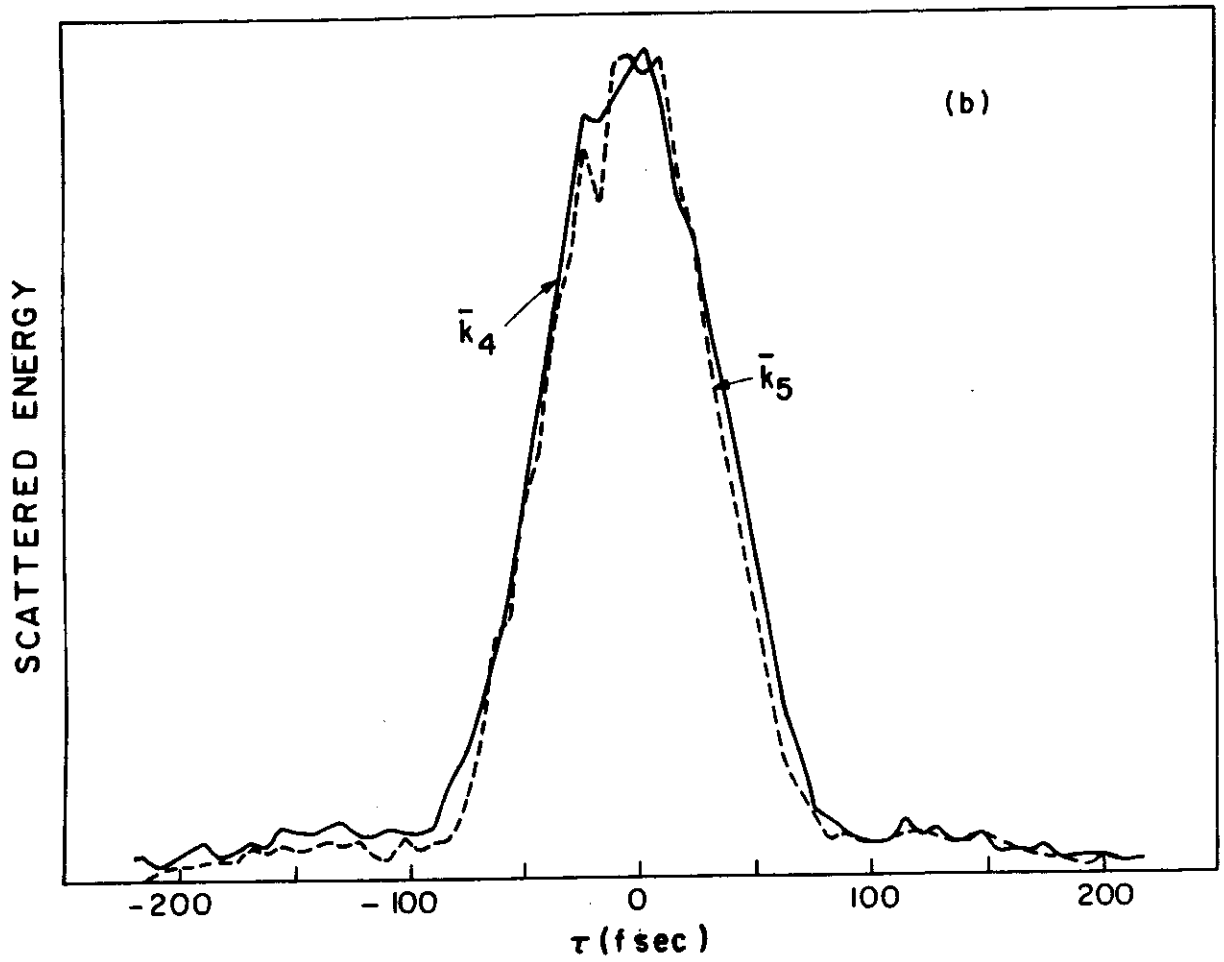

Fig. 9b

64

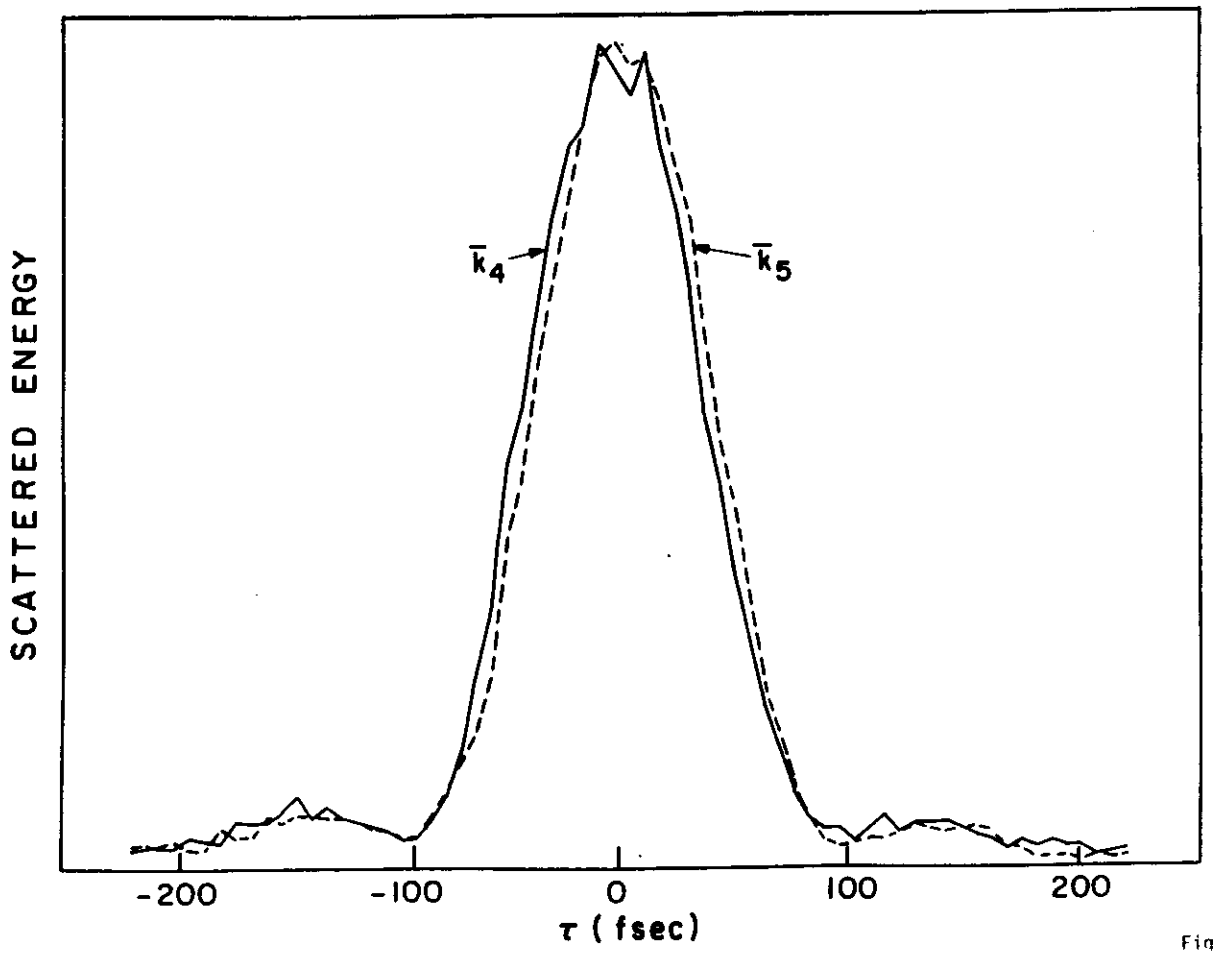

Fig. 10

65